Simulation of hydrodynamic forces on an eccentric whirling cylinder

Knoors, E.M.H.

Award date:
1995

Shell Research

Rijswijk

Simulation of hydrodynamic forces on an eccentric whirling cylinder

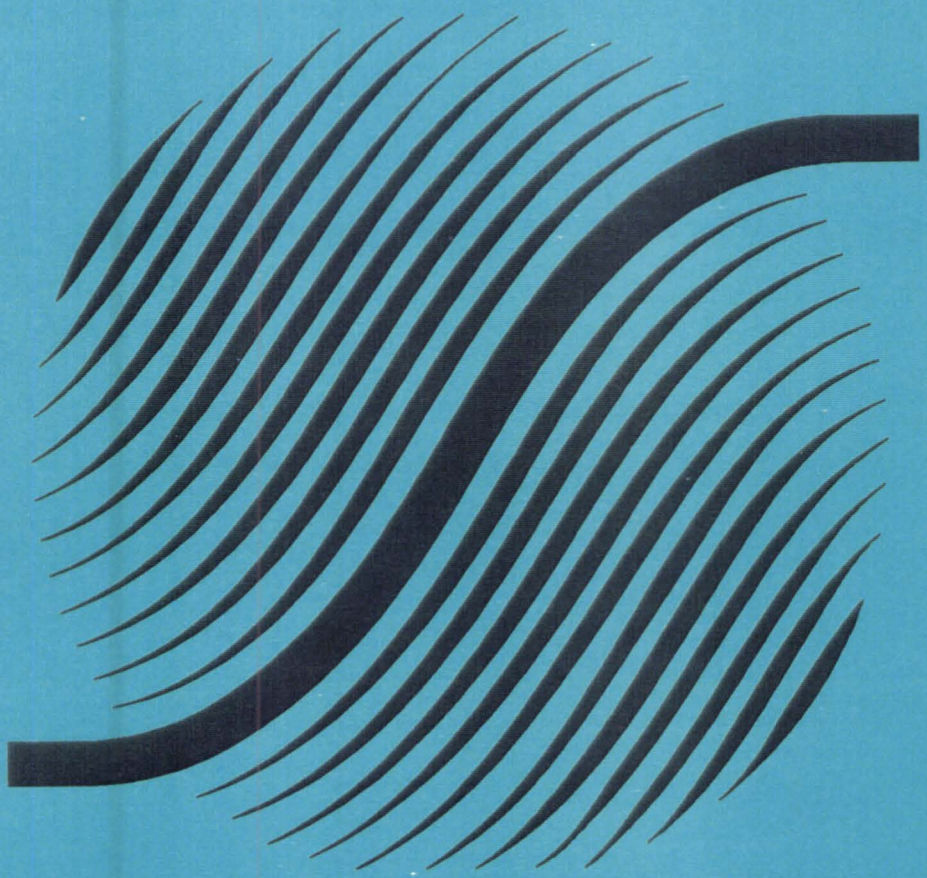

By
Ernest Knoors
august 1995

Technische Universiteit tu/e Eindhoven

Vakgroep Transportfysica
Faculteit Technische
Natuurkunde
Gebouw W&S
Postbus 513
5600 MB Eindhoven

Titel: .Simulation of hydrodynamic forces on an eccentric whirling cylinder

Auteur: .E. Knoors

Verslagnummer: .R-1358-A

Datum: .Augustus 1995

Werkeenheid: .Werveldynamica

Begeleider(s): .prof.dr.ir. G.J.F. van Heijst
dr. H.J.H. Clercx

Summary

While drilling for oil and gas, drilling mud is circulated from the surface to the bottom of the hole. This fluid maintains the correct pressure in the hole, cools the bit, and transports the cuttings to the surface. Due to the rotating and whirling motion of the drillstring the fluid will flow in a spiralling manner in the annulus between drillstring and borehole wall. The resulting hydrodynamic force, which can be decomposed in a lift and a drag force, influence the drillstring dynamics.

To study these forces a two dimensional model has been developed, consisting of a whirling rotor confined in a stator. The model is fully characterized by four non dimensional parameters: the eccentricity ε, the ratio of the rotor and stator radii η, the ratio of rotational and whirling velocity γ, and the Taylor number Ta. The main difference between model and actual field situation is in assuming a Newtonian fluid, neglecting axial flow and lower rotational velocities.

Previous research has been limited to small eccentricity values. The present study is the first, as far as we know, to solve the flow problem for the complete eccentricity range (ε=0-0.9) as well as examining the influence of η, γ and Ta on the flow and the hydrodynamic force.

The flow was simulated using the numerical code FLUENT V4.2 based on a finite difference method. This program can create plots of the stream function and pressure distribution in the annulus, and calculate the forces on the rotor. For turbulent flow it also provides plots of the turbulent kinetic energy distribution.

On the basis of these plots the flow in the annulus surrounding an eccentric whirling rotor has been studied. The case of concentric cylinders was also considered. The influence of the four non-dimensional parameters on the torque, lift and drag force has been examined.

This report is a condensed version of a confidential report which contains all the quantative results. The confidential version is kept in the library of the KSEPL in Rijswijk.

Table of contents

Acknowledgments

This report has been written as part of my graduation work during a period of ten months at Shell Research in Rijswijk (KSEPL). I would like to thank my mentors, Bettina Kampman and dr. Herman Clercx, for their advice and guidance. Furthermore I would like to express my gratitude to Prof. GertJan van Heijst at Eindhoven University of Technology for giving me the opportunity for this external graduation project. It is my opinion that the experience of a traineeship in a company as Shell is of immense value to the schooling of engineers and should be a part of every students curriculum.

A big word of thanks goes out to Mathieu Molenaar, Marco den Burger, Arjen Smit, Simon Angove and my other student colleagues. Their presence in and outside of KSEPL has truly made my stay a period to remember and I wish them all the best in their pursuit of "love and happiness". Many thanks also to a very special group of students of which I am proud to be a part, better known as Cavedudes, for just being the dudes they are.

Last but not least I would like to thank my brother and parents for their support during the entire period of my education.

List of symbols

Symbol	Description	Dimension
Lower case		
a	Cell aspect ratio	[-]
d	Displacement of the rotor relative to O	[m]
k	Turbulent kinetic energy	[J]
p	Pressure	$[Nm^{-2}]$
r	Radial coordinate	[-]
t	Time	[s]
v	Velocity	[m/s]
v'	Velocity in rotating reference frame	[m/s]
x	1st coordinate in cartesian space in inertial reference frame	[-]
x'	1st coordinate in cartesian space in rotating reference frame	[-]
y	2nd coordinate in cartesian space in inertial reference frame	[-]
y'	2nd coordinate in cartesian space in rotating reference frame	[-]
z	3rd coordinate in cartesian space in inertial and rotating reference frame	[-]
Upper case		
A	Rotor surface	$[m^2]$
C	Annulus width $R_o - R_i$	[m]
$C_{loc.}$	Local annulus width	[m]
C_D	Drag coefficient	[-]
C_L	Lift coefficient	[-]
C_M	Torque coefficient	[-]
I	1st coordinate in computational domain	[-]
J	2nd coordinate in computational domain	[-]
O	Stator center	[-]

O'	Rotor center	[-]
R_i	Radius of rotor	[m]
R_o	Radius of stator	[m]
Ta, Ta_{glob}	Global Taylor number	[-]
$Ta_{loc.}$	Local Taylor number	[-]
$Ta_{crit}, Ta_{glob.crit}$	Critical global Taylor number	[-]
$Ta_{loc.crit.}$	Critical local Taylor number	[-]
$U_{\tan}, U_\theta$	Tangential velocity	[m/s]
$U_{rad.}, U_r$	Radial velocity	[m/s]

Lower case greek

θ	Angular coordinate	[-]
ε	Dissipation rate of turbulent kinetic energy	[J/s]
ε	Eccentricity $d/(R_O - R_i)$	[-]
ϕ	Angle relative to positive y axis	[rad]
ϕ_n	Modal shape of a lateral vibration	[-]
γ	Ratio of ω and Ω	[-]
η	Ratio of R_i and R_o	[-]
μ	Molecular viscosity	[Pas]
μ_{eff}	Sum of turbulent and molecular viscosity	[Pas]
μ_t	Turbulent viscosity	[Pas]
ν	Kinematic viscosity	[m^2/s]
ω	Rotational velocity of rotor around O'	[rad/s]
ρ	Density	[kg/m^3]
ρ_w	Density of water	[kg/m^3]
τ	Stress tensor	[Pa]

Upper case greek

Ω	Whirling velocity of rotor around O	[rad/s]
Ω_n	Natural circular frequency of lateral vibration	[rad/s]

Miscellaneous symbols

∂	Partial differential operetor	[-]
∇	Differential operator	[-]

Chapter 1. Introduction

1.1 Introduction

Drilling for oil and gas is an expensive and highly complex process. The main objective of research at KSEPL is to make this process more efficient. The subject of research in this study is drill string dynamics, more specifically the interaction between drilling fluid and drill string. We will start the present chapter by giving a short explanation of the general process of oil well drilling (section 1.2). We will then proceed to discuss drill string dynamics in section 1.3. Finally in section 1.4 and 1.5 the objectives and motivation for the study are given as well as a short outline of the organisation of the chapters.

1.2 Rotary drilling

The main process during deep well drilling for oil or gas is the creation of a borehole by a rock-cutting tool called a bit. For this process two transport flows are required: energy transport from the surface to the bit, and material transport from the bit to the surface. The drilling technique commonly used in the oil industry, called rotary drilling, relies on a combined mechanical/hydraulic system for energy and material transport (see figure 1.1). The mechanical part is composed of a rotating bit to generate the borehole, a drill string to rotate the bit, a rotary drive at the surface to rotate the drill string, and a rig to support the string and the rotary drive. The hydraulic part consists of mud (drilling fluid), pumps and a transport channel: the mud is pumped down through the drill string and flows back through the annulus between the drill pipe and the borehole wall. The upper part of the borehole wall is supported with casings. The drilling fluid usually consists of water with viscosifiers and weighting materials, and is strongly non-Newtonian (shear thinning). It aids the cutting process by a jetting action, it cools and lubricates the bit and transports the cuttings from the hole bottom to the surface. The cuttings are separated from the mud in a solids-removal system which consists of sieves, cyclones and centrifuges.

The drill string consists mainly off drill pipes: slender tubes, about 9 m long, coupled with threaded connections, with an outside diameter of 127 mm (5 in.), and a wall thickness of 9 mm. The lowest part of the drill string, the bottom hole assembly (BHA), is loaded in compression. To avoid buckling the BHA consists of thick wall tubulars, called drill collars, and stabilisers. The BHA can be several hundred meters long and contains besides the drilling bit several specialised tools.

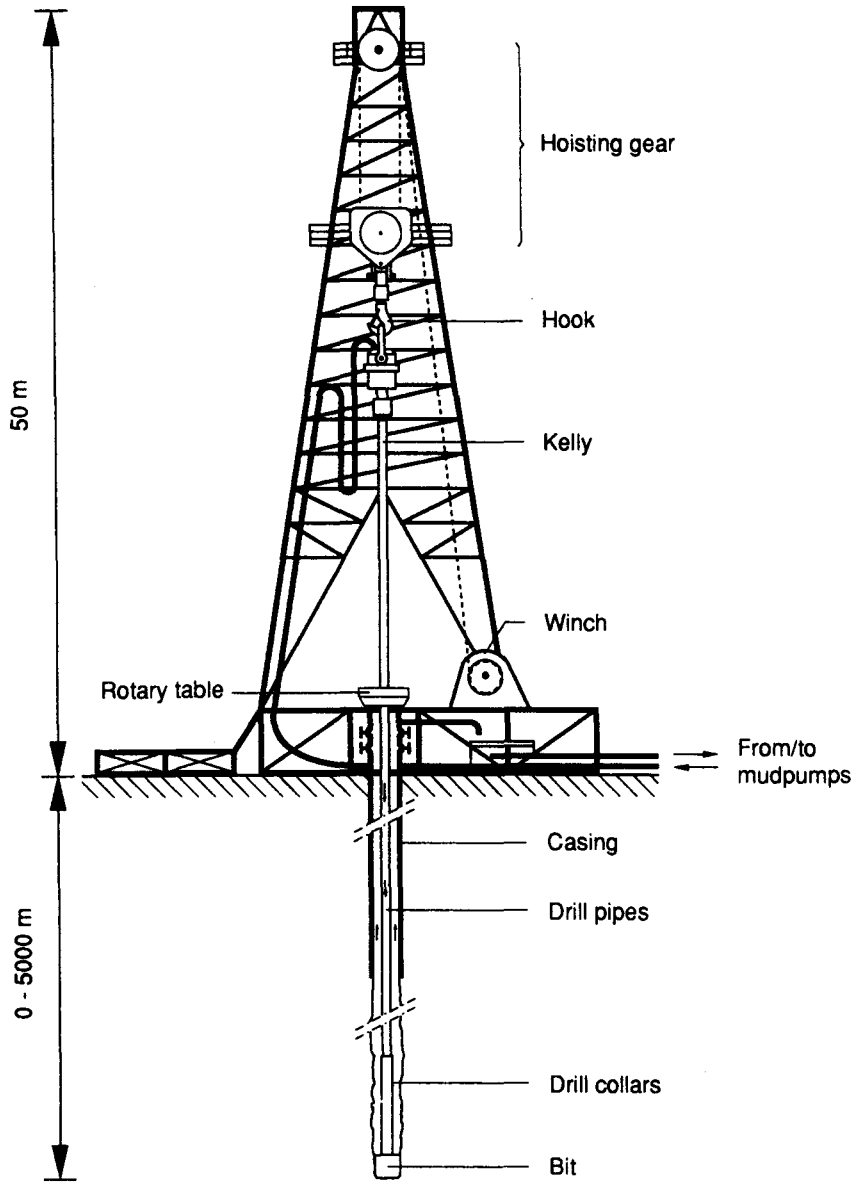

Figure 1.1: Essential components of an oil well drilling rig

The drill string is rotated by the rotary table and a motor at the surface thus enabling the actual drilling by the bit. Another way of generating rotation of the bit is by using a downhole motor (Moineau motor). In that case the energy flow to the bit mainly stems from the mud flow and only a small part from the rotation of the drill string.

1.3 Drill string dynamics

This section discusses the different types of vibrations which can occur when operating a drill string, and the resulting whirling motion of the drill string. The hydrodynamic force acting on the drill string due to its motion is also discussed.

1.3.1 Drill string vibrations

A drill string is an extremely slender structure with a ratio between length and diameter larger than that of a human hair. Because the string has a diameter smaller then the borehole it is free to vibrate laterally. These lateral or bending vibrations are especially important in the lower part of the drill string. Higher up, the tension in the drill string causes the string to be in continuous contact with the borehole wall in most places, because boreholes are always slightly curved. This kind of vibration is very difficult to detect at the surface and as a result it has been overlooked for a long time. An important cause of lateral vibrations are out-of-balance forces in drill collars, resulting in a whirling motion, just as in an unbalanced centrifuge. Another cause of lateral vibration is the friction between the rotating drill string and the borehole wall, which can produce a backward rolling motion of the drill string along the wall. Other types of vibrations which can occur in a drill string are torsional vibrations (stick-slip) and longitudinal vibrations (bit bounce). These are both of less importance to us now.

1.3.2 Drill string motion

Without going into the details of the complex equation of motion for a drill string we will discuss now the basic motion of a section of drill collar between two stabilisers. More details are given in work by Jansen [JAN 1993] and Axisa et al. [AXI 1991]. As mentioned above drill collars can perform a lateral or bending vibration (see figure 1.2).

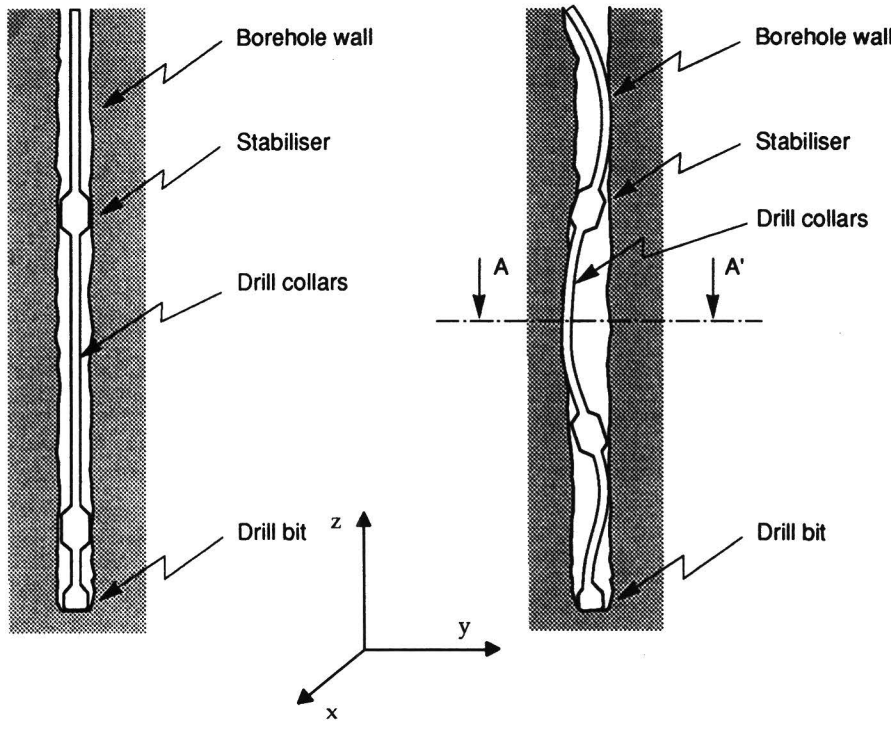

Figure 1.2: Schematic view of a straight and lateral vibrating drill collar

If we now consider the zy plane the vibration is described by

$$\phi_n(z)e^{i\Omega_n t} \tag{1.1}$$

where ϕ_n is a real modal shape and Ω_n a positive natural circular frequency of vibration. The same vibration will be present in the zx plane. Combining the two motions will result in a circular motion around the centre of the borehole at a circular frequency Ω_n (see figure 1.3 a) This motion is called the whirling motion of the drill string. Besides this whirling motion the drill string also rotates at a circular frequency ω for the actual drilling. Thus the resulting motion will consist of two rotations as depicted in figure 1.3 b. The rotation is defined positive in the counter clockwise direction.

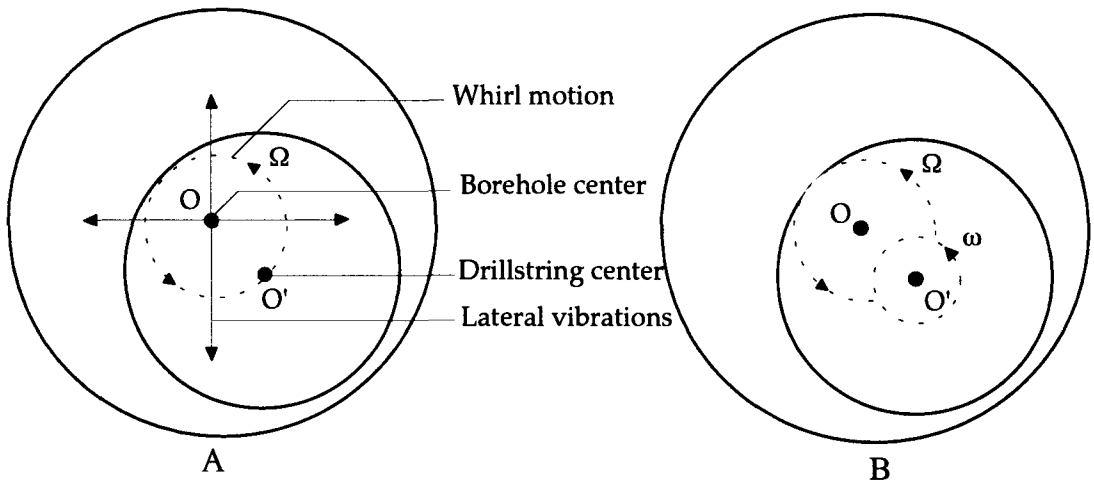

Figure 1.3 a: Whirling motion of drill string, b Total motion of the drill string

If the ratio of the rotational velocities $\gamma=\omega/\Omega$ is negative the drill string will role or slip along the borehole wall. This motion is called backward whirl. The case of positive γ is called forward whirl.

1.3.3 Hydrodynamic forces

Due to the motion of the drill string as discussed above the drilling fluid will exert a force on the string which can be decomposed into a drag force and a lift force. The lift force is defined as the force increasing the eccentricity of the drill string. The drag force is defined as the force opposing the whirl motion of the drill string (see figure 1.4)

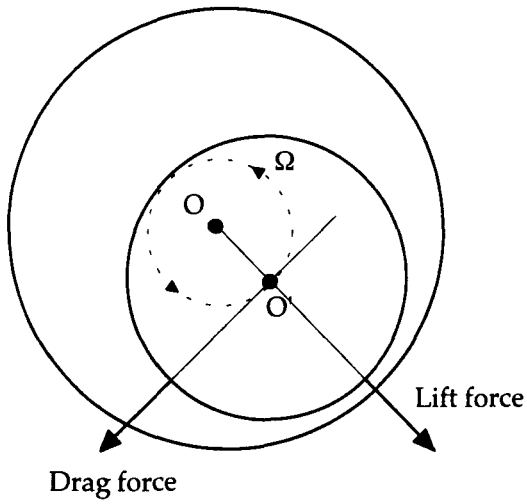

Figure 1.4: Definition of the hydrodynamic forces

1.4 Objectives and motivation of research

Drill string vibrations are an important cause of premature failure of bits, downhole motors and other drill string components. When a crack in the drill string is detected while drilling the string has to be removed from the hole to exchange the failed component. When the crack is not detected it may result in parting of the drill string, and after removing the top part of the string the remaining part has to be fished out of the hole with special equipment. In the worst case the bottom part of the string is not recovered, expensive equipment is lost and a part of the hole has to be abandoned. At best costly drilling time is wasted. Thus reducing or controlling drill string vibrations is a very important factor in improving drilling technique. From literature [WAL 1964] it is known that the lift and drag force influence the critical rotational velocity of a rotating shaft, i.e. velocity for which large lateral vibrations occur, and the amplitude of these vibrations (see figure 1.5).

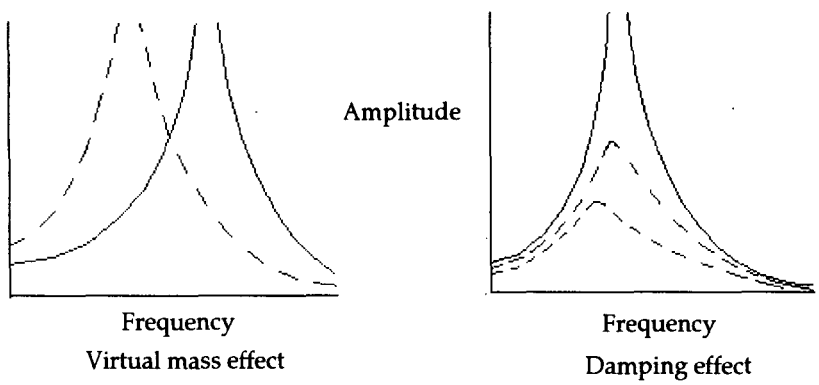

Figure 1.5: Effects of virtual mass (lift force) and fluid damping (drag force) on lateral vibrations. Dashed lines represent fluid effects

The hydrodynamic forces on a drillstring have not yet been investigated. The objective of this study is to develop a program which can provide us with information on these forces. Combined with experiments which are currently being developed this will hopefully lead to a better insight in the influence of the hydrodynamic forces on drill string vibrations.

1.5 Outline of report

The report is based on work performed at the Koninklijke/Shell Exploratie en Produktie Laboratorium (KSEPL) during the past 10 months

In chapter 2, the actual field situation is translated into a model which can be used in the simulations. This chapter also contains a short review of relevant literature. Chapter 3 contains information about the numerical simulation program FLUENT V4.2 with which the simulations were performed. In chapter 4 the results of the simulations are presented which will be discussed in chapter 5 along with some key issues about the simulation (grid independence, non-dimensional parameters and Taylor number). Finally in chapter 6 a summary of the conclusions is given along with recommendations for future research.

Chapter 2. Formulation of the problem

2.1 Introduction

Having considered the principles of drilling for oil and the general drillstring dynamics we will now consider a simplification of the present problem which will be the subject of this study. The field situation described in section 2.2 is translated into a model in section 2.3. This model enables us to evaluate the fluid forces by numerically simulating the flow. Non-dimensional parameters will be derived for the model and the different flow regimes in the annulus will be discussed. In section 2.4 a review of the relevant literature on the problem is presented followed by a brief outline of the simulations in section 2.5.

2.2 The situation in the field

The equipment and principles of drilling have already been discussed in chapter 1. A short recapitulation is given in order to compare the actual situation to the model. Consider a horizontal cross section of a borehole assembly (see figure 2.1).

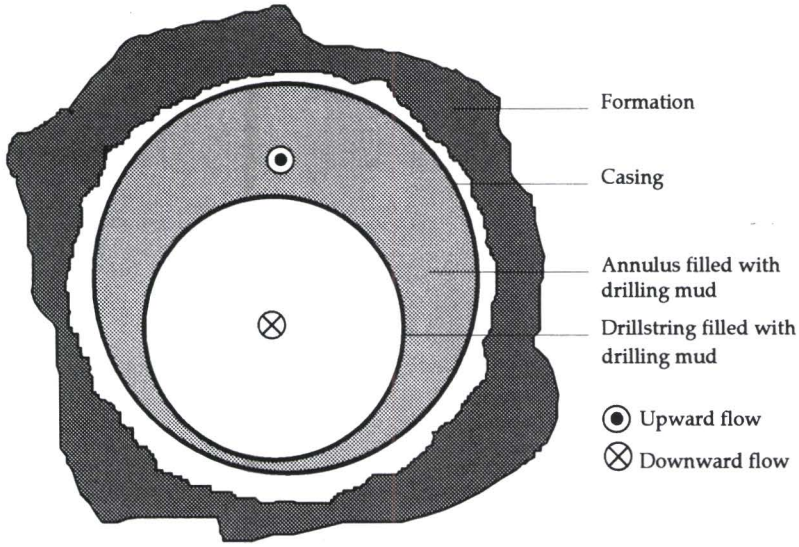

Figure 2.1: Cross section of a borehole

The actual borehole as drilled by the bit in the formation will be rough surfaced. For the upper part of the hole casings will be inserted in the borehole as mentioned in chapter 1. In the lower part of the borehole however no casings are used. The borehole wall is covered with filter cake, a thick sticky mud. Once the drill string touches the borehole

wall large forces must be exerted on the string to pull it free from this cake. Mud is pumped down into the borehole through the drill sting and is transported up out of the borehole through the annular space between drill string and casing or borehole wall. The drill string performs either a forward or backward whirling motion in the borehole as explained in chapter 1. The rotational velocity of the drill string can vary between 100 and 300 rpm.. The resulting flow in the annulus of the non-Newtonian mud, which contains cuttings and gas bubbles, will be a turbulent spiral motion.

2.3 A two dimensional model of the problem

From the description in the previous section it can be concluded that the problem in the field is very complex. In order to be able to simulate the flow and calculate the hydrodynamic forces numerically we will have to simplify the situation considerably. The assumptions made in the model are discussed in section 2.3.1. In section 2.3.2 four non-dimensional parameters which characterise the flow problem are presented together with the scaling factors for torque and force. In Section 2.3.3 we will briefly discuss the possible flow regimes in the annulus as a function of the Taylor number.

2.3.1 The assumptions

Figure 2.2 shows the 2D model for the problem including the definition of the forces and some of the symbols. The vectors are all positive in the directions shown. The torque is defined positive in the direction opposing the rotation of the rotor.

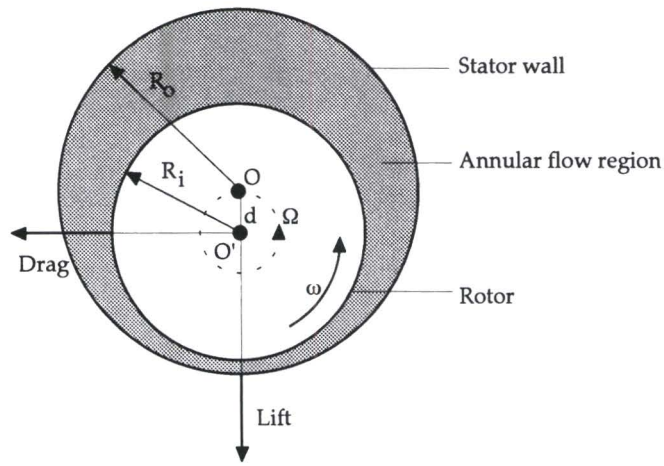

Figure 2.1: Schematic representation of the two dimensional model

In the model, the borehole and drillstring are represented by a stator and a rotor, respectively. The force and torque will be considered per unit length of the rotor. The surface of these objects are assumed to be perfectly smooth. The radii of the stator and rotor, R_o and R_i respectively, are based on a five inch diameter drill string within an eight inch diameter casing. However R_i is increased in the simulations up to a value of 3.6 inch. In the model the annulus is filled with water, which does not contain any cuttings or gas. The presence of the filter cake is also neglected. The flow in the annulus

is taken to be strictly two dimensional so axial flow is not considered. Four different whirl motions are simulated with rotational velocities varying between 0.008 rad/s and 0.5 rad/s. Table 2.1 compares the model to the field situation and figure 2.3 shows the four different whirl motions which will be considered in the simulations.

	Field situation	Model
Wall roughness	Yes	No
Radius casing (R_o)	3.5-15 inch	4 inch
Radius drillstring (R_i)	2.5 inch	2.5, 2.8, 3.6 inch
Drilling mud	non-Newtonian	Newtonian (water)
Rotational velocities	10-30 rad/s	0.008-0.5 rad/s
Flow	3 dimensional	2 dimensional
Flow regime	turbulent	laminar/turbulent
Whirl motion	Yes	Yes

Table 2.1: Comparison of model and field situation

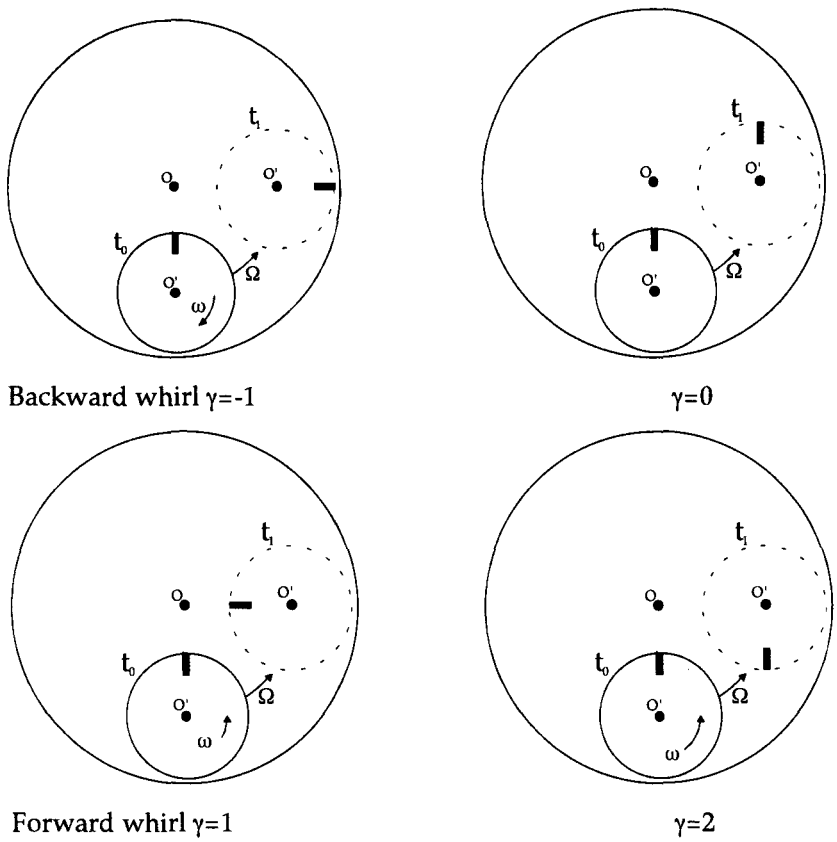

Figure 2.3: Four different whirl motions considered in this study

In each plot in figure 2.3 the position of the rotor is depicted for two points in time t_0 and t_1. A marker is drawn on the rotor which enables the reader to distinguish the rotor motion more clearly. The rotor size has been down scaled for clarity.

2.3.2 *The non dimensional parameters*

The non-dimensional parameters for a flow problem can be derived from the dimensional parameters by using the Buckingham's pi theorem [KUN 1990]. The present flow model is described by seven independent parameters: inner and outer radius R_i, and R_o, respectively, the displacement of the rotor centre relative to the stator centre d, the rotational and whirl velocity of the rotor ω and Ω, respectively, the fluid density ρ and the dynamic viscosity μ. This is reduced to a total of four non-dimensional parameters which are given in table 2.2 along with their definition

Non dimensional parameter	Definition
ε	$\frac{d}{R_O - R_i}$
η	$\frac{R_i}{R_o}$
γ	$\frac{\omega}{\Omega}$
Global Taylor number Ta	$\frac{\omega\rho R_i\left(R_O - R_i\right)}{\mu}\sqrt{2\frac{\left(R_O - R_i\right)}{R_o + R_i}}$

Table 2.2: Non-dimensional parameters

In order to be able to compare the results to other cases they have to be non-dimensionalized. In this study this was achieved by using the scaling factors in Table 2.3 keeping in mind that the force and torque are considered per unit length of the rotor.

Non-dimensional coefficients	Scaling factor
Torque C_M	$\frac{1}{2}\pi\rho(\omega R_i)^2 R_i^2$ [N]
Drag force C_D	$\rho(d\Omega)^2 R_i$ [N/m]
Lift force C_L	$\rho\pi R_i^3\Omega^2$ [N/m]

Table 2.3: Scaling factors

2.3.3 *The flow regimes*

The basic flow regimes, which can be present in an annulus between a whirling rotor and a stator, can best be discussed by considering two concentric cylinders of which only the inner one is rotating. This case has been subject of many studies [TAY 1923],[KAT 1984]. The flow for low rotational velocity is a shear flow without a pressure gradient in the direction of mean flow. When the rotation speed of the inner cylinder is increased beyond a critical value the basic laminar axi-symmetric flow, known as Couette flow, becomes unstable. The centrifgal instability leads to a transition to a laminar cellular vortex flow, referred to as Taylor vortex flow. The vortices rotate in alternately opposite directions around axes which are located along the circumference of the inner cylinder (see figure 2.4)

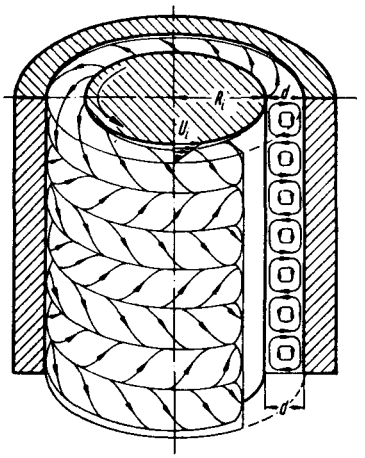

Figure 2.4: Taylor vortices between two concentric cylinders of which the inner one is rotating.

The conditions for the laminar Couette flow to become unstable can be expressed by a characteristic number known as Taylor number, Ta, of the form as given in table 2.2. If the rotational velocity is further increased the height of the vortex cells will reduce and eventually disappear. The flow is then fully turbulent.

In all, we may discern three flow regimes, each circumscribed by the Taylor number in the following way

Ta < 41.3: laminar Couette flow

41.3 <Ta< 400 : laminar flow with Taylor vortices

Ta> 400: turbulent flow

These critical numbers are only valid for the concentric case. It will be seen that a global Taylor number as used here is not accurate in predicting flow for an eccentric whirling rotor (section 5.3) An important point is brought up by this discussion. The model as defined in this section assumes two dimensionality, and since Taylor vortex flow is obviously three dimensional this cannot be simulated by the model.

2.4 A literature survey

The case of two concentric cylinders, with the inner one rotating, has been the subject of numerous studies. Thus there is no problem in comparing data from simulations and literature. For this purpose we will use data from Schlichting's book on Boundary-Layer Theory [SCH 1979]. Although literature concerning whirling rotors is very limited several studies have been found which contain relevant data.

Two articles written by Iida [IID 1956],[IID 1959] deal with the problem of a confined and a non-confined whirling rotor. In these articles the hydrodynamic force is calculated from the equation of motion expressed in terms of the stream function. The whirl amplitude is assumed to be small $\frac{d}{R_i} << 1$. The resulting equations are then solved by using power series expansions. Lift and drag forces are plotted for several $\eta = \frac{R_i}{R_o}$ values and eccentricities. A limited number of experiments (only two as far as we know) were carried out, again for small ε, to support the results of Iida.

Another paper on the subject by R. J. Fritz [FRI 1970] consists of a theoretical part and an experimental part. In the theoretical part expressions are derived for the hydrodynamic force for Taylor vortex flow and for turbulent flow by using fluid friction factors in the continuity and momentum equation. Fritz limited his approach to small eccentricities. The results are supported by an extensive set of experiments.

"On the flow in an annulus surrounding a whirling cylinder" written by C. Brennen [BRE 1976] is an article in which general solutions of the Navier-Stokes equations are presented. These solutions are limited to a small amplitude of the whirl motion thus allowing a linearization of the equations. From these solutions the hydrodynamic force is derived under a wide variety of circumstances, including large and small annular widths and high and low Reynolds numbers. Expressions for the actual forces are given only for the limiting cases such as inviscid and laminar flow. No experiments were carried out to support the theory but the results are in good agreement with Fritz' results.

Research has been carried out concerning journal bearings [SHA 1949] which can display the same whirling motion, particularly dynamically loaded bearings, but is essentially different from our case. In journal bearing theory η is considered to be almost unity thus flow in the radial direction can be neglected. The equation describing the flow in these thin lubrication films is called the Reynolds equation. It has been demonstrated by Wannier [WAN 1950] that this Reynolds equation is a first order approximation for the Stokes equations if all quantities are expanded in powers of film thickness. Lubrication theory is therefore not applicable in our study because of the large film thickness ($\eta \sim 0.7$) and results can not be compared. However some basic features of lubrication theory can be used in discussing the flow in the narrow annulus region for large ε.

2.5 Outline of simulations

Up until now the problem of whirling flow has only been solved for small eccentricity. The present study is the first, as far as we know, to solve the problem for the whole eccentricity range (ε=0-0.9) as well as examining the influence of the non-dimensional parameters η, γ and Ta. This provides a more accurate and complete insight in the hydrodynamic force and torque on the rotor. The simulations used for these purposes can be divided in three categories

- The concentric case. The torque calculated from these simulations can be compared with experimental data obtained from the literature. This way we can get an impression of the accuracy and validity of the method for both laminar and turbulent flow

- The case of laminar whirl motion. These simulations are the first step in simulating the actual flow field. The force and torque on the rotor are determined and the influence of the parameters ε, η and γ is studied.

- The case of turbulent whirl motion. Again the force and torque on the rotor are determined and the influence of the parameters ε and γ is studied.

The results of these simulations are given in chapter 4 and will be compared to data found in literature in chapter 5. Further simulations have been carried out to check the grid independence of the method. Whether the non-dimensional parameters and scaling factors characterise the flow problem correctly has also been checked. These results are also discussed chapter 5

Finally it should be mentioned that the model as discussed in this chapter is in no way an accurate representation of the field situation. It does however provide a good insight in the basic fundamentals of the annular flow. It is possible to extend the model to contain non-Newtonian fluids, axial flow and two phase flow. Thus it provides a good fundamental basis for further research.

Chapter 3 The simulation

3.1 Introduction

The simulations were performed with the FLUENT V4.2 code which is a general purpose computer program for modelling fluid flow, heat transfer and chemical reaction. This wide range of phenomena is modelled by solving the conservation equations for mass, momentum and energy using a control volume based, finite difference method. The governing equations are discretized on a curvilinear grid. The basic structure of this code and the theoretical basis will be discussed in section 3.2. The way in which the two dimensional model is implemented in the code is the subject of section 3.3 where features like the geometry, the boundary conditions and the grid are considered. Finally the solution method in FLUENT is explained in section 3.4, dealing with the control volume technique, the discretization procedures, the SIMPLEC algorithm and the iterative solution procedure.

3.2 The code FLUENT V4.2

The program FLUENT V4.2 consists of two basic parts, the pre-processor preBFC V4, and a main module FLUENT as shown in figure 3.1. In preBFC V4 the geometry and a structured grid for the model are generated. The grid information is then transferred from preBFC to FLUENT via a grid file. Following this transfer, FLUENT can be used to define physical models, fluid properties and boundary conditions that describe the problem. This information is added to the grid information and stored in a case file which is a record of all the input for the problem definition. All calculations and post processing are performed in FLUENT and the results are stored in a data file.

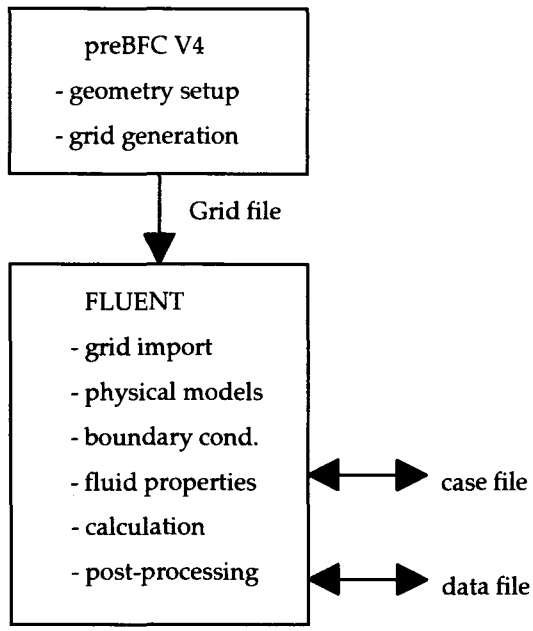

Figure 3.1: FLUENT V 4.2 basic program structure

Although FLUENT solves all equations in general curvilinear coordinates all equations in the remainder of this chapter are introduced in Cartesian tensor form for simplicity. The standard summation convention will be used.

The equations describing laminar flow are based on

- conservation of mass
- conservation of momentum
- conservation of energy

Only the first two conservation laws will be considered since the conservation of energy is of no interest to our problem. Conservation of mass expressed by the continuity equation yields:

$$\frac{\partial \rho}{\partial t} + \frac{\partial}{\partial x_i}\left(\rho u_i\right) = 0 \tag{3.1}$$

Conservation of momentum in the i^{th} direction in an inertial (non accelerating) reference frame is described by

$$\frac{\partial}{\partial t}\left(\rho u_i\right) + \frac{\partial}{\partial x_j}\left(\rho u_i u_j\right) = -\frac{\partial p}{\partial x_i} + \frac{\partial \tau_{ij}}{\partial x_j} + \rho g_i + F_i \tag{3.2}$$

where p is the static pressure, τ_{ij} is the stress tensor (described below) and g_i and F_i represent the gravitational acceleration, which can be neglected, and external body forces. This last term is used to account for the rotation of the reference frame as

described below. Furthermore the flow is assumed to be incompressible. The stress tensor is then given by:

$$\tau_{ij} = \mu\left(\frac{\partial u_i}{\partial x_j} + \frac{\partial u_j}{\partial x_i}\right) \tag{3.3}$$

where μ is the molecular viscosity.

FLUENT also allows computation of flows in a rotating reference frame as we will use in the solution of our problem. Since a rotating coordinate system is a non-inertial accelerating reference frame, body force terms arise in the momentum equation 3.2, where the acceleration of the fluid is augmented by the angular acceleration of the reference frame. The total acceleration of the fluid in a constant rotating frame is thus:

$$\frac{Dv}{Dt} + 2\Omega \times v + \Omega \times (\Omega \times r) \tag{3.4}$$

Here, v is the velocity in the rotating frame and is related to the velocity in the non-rotating frame, v', as:

$$v' = v + \Omega \times r \tag{3.5}$$

where Ω is the rotation vector and r is the position in the rotating frame. Thus, when a problem is defined in a rotating reference frame FLUENT solves the velocity relative to the rotating reference frame. This should be kept in mind when examining the stream functions in chapter 4.

Having considered the basic equations for laminar flow we now proceed to discuss the turbulence model as used in FLUENT. The conservation equations used in FLUENT for turbulent flows are obtained from those of the laminar flows using a time averaging procedure commonly known as Reynolds averaging. This averaging procedure for scalar equations can be illustrated using a transport equation for a conserved scalar quantity φ:

$$\frac{\partial}{\partial t}(\rho\phi) + \frac{\partial}{\partial x_i}\left(\rho u_i \phi\right) = D_\phi + S_\phi \tag{3.6}$$

Accumulation Convection Diffusion Source

The value of φ in turbulent flow can be decomposed into a mean value and a fluctuating part:

$$\phi = \bar{\phi} + \phi' \tag{3.7}$$

where $\bar{\phi}$ is the time averaged value of ϕ defined as :

$$\bar{\phi} = \frac{1}{\Delta t}\int_0^{\Delta t} \phi dt \tag{3.8}$$

and Δt is a time scale much larger than the largest time scale of turbulent fluctuations. Turbulent fluctuations are assumed to be random such that

$$\overline{\phi'} = 0 \tag{3.9}$$

Substitution of 3.7, together with analogous decompositions of u_i, D_ϕ and S_ϕ, in the general conservation equation 3.6 and time integration over a sufficiently large time interval yields

$$\frac{\partial}{\partial t}(\bar{\phi}) + \frac{\partial}{\partial x_i}\left(\bar{u}_i\bar{\phi}\right) = -\frac{\partial}{\partial x_i}\left(\overline{u_i'\phi'}\right) + \frac{1}{\rho}\left[\bar{D}_\phi + \bar{S}_\phi\right] \tag{3.10}$$

The terms in 3.10 are similar to those in its laminar flow counterpart (eq. 3.6) except that each quantity now is represented by its time averaged value and a new term containing the correlation $\overline{u_i'\phi'}$ appears on the right-hand side. This term multiplied by ρ represents the diffusion of ϕ due to turbulent fluctuations. In the momentum equation, the double correlation $\overline{u_i'\phi'}$ becomes $\overline{u_i'u_j'}$. Note that $\overline{u_i'u_j'}$ is a symmetric second order tensor and hence has six unique terms. These terms, multiplied by the density are known as the Reynolds stresses. Expressions for the Reynolds stresses are obtained, in our case, via the k-ε model

The k-ε turbulence model is an eddy viscosity model in which the Reynolds stresses are assumed to be proportional to the mean velocity gradients, with the constant of proportionality being the turbulent eddy viscosity μ_t. This assumption provides the following expression for the Reynolds stresses:

$$\rho\overline{u_i'u_j'} = \rho\frac{2}{3}k\delta_{ij} - \mu_t\left(\frac{\partial\bar{u}_i}{\partial x_j} + \frac{\partial\bar{u}_j}{\partial x_i}\right) \tag{3.11}$$

where k is the turbulent kinetic energy:

$$k = \frac{1}{2}\sum_i \overline{u_i'^2} \tag{3.12}$$

The equation for the Reynolds stresses is analogous to that describing the shear stresses that arise in laminar flow with the turbulent viscosity μ_t playing the same role as the molecular viscosity μ Therefore the form of the turbulent momentum equations remain identical (neglecting the first term on the right hand side in eq. 3.11 because it represents the turbulent pressure which is in general much smaller than the static pressure) to the form of the laminar momentum equations except that μ is replaced by an effective viscosity μ_{eff};

$$\mu_{eff} = \mu + \mu_t \tag{3.13}$$

The turbulent viscosity is obtained by assuming that it is proportional to the product of a turbulent velocity scale and length scale. In the k-ε model, these velocity and length scales are obtained from two parameters: k the turbulent kinetic energy and ε the dissipation rate of k. Thus

$$\mu_t = \rho C_\mu \frac{k^2}{\varepsilon} \tag{3.14}$$

where C_μ is an empirically derived constant (set to a default value of 0.09 in FLUENT) The values of k and ε required in equation 3.14 are obtained by solution of the following conservation equations

$$\frac{\partial}{\partial t}(\rho k)+\frac{\partial}{\partial x_i}\left(\rho u_i k\right)=\frac{\partial}{\partial x_i}\left(\frac{\mu_t}{\sigma_k}\frac{\partial k}{\partial x_i}\right)+G_k-\rho\varepsilon$$
$$\frac{\partial}{\partial t}(\rho \varepsilon)+\frac{\partial}{\partial x_i}\left(\rho u_i \varepsilon\right)=\frac{\partial}{\partial x_i}\left(\frac{\mu_t}{\sigma_\varepsilon}\frac{\partial \varepsilon}{\partial x_i}\right)+C_{1\varepsilon}\frac{\varepsilon}{k}G_k-C_{2\varepsilon}\rho\frac{\varepsilon^2}{k} \quad (3.15)$$

where $C_{1\varepsilon}$ and $C_{2\varepsilon}$ are empirical constants,σ_k and σ_ε are "Prandtl" numbers governing the turbulent diffusion of k and ε and G_k is the rate of production of turbulent kinetic energy:

$$G_k=\mu_t\left(\frac{\partial u_j}{\partial x_i}+\frac{\partial u_i}{\partial x_j}\right)\frac{\partial u_i}{\partial x_j} \quad (3.16)$$

Details of the assumptions involved in the k-ε model description provided here can be found in [ROD 1984]. The values of the empirical constants as used in the simulations by FLUENT are given in table 3.1

Constant	Value
C_μ	0.09
σ_k	1.0
σ_ε	1.3
$C_{1\varepsilon}$	1.44
$C_{2\varepsilon}$	1.92

Table 3.1: Constants in FLUENT's k-ε turbulence model [FLU 1993]

From previous publications [ROD 1984], [SCH 1979] the k-ε model is known to be applicable for pipe and annular flow. The basic restriction on this model being that the turbulent fluctuations are assumed to be isotropic. The use of other, more accurate turbulence models like the Reynolds Stress Model or the Renormalized Group Model is possible in FLUENT. The k-ε was chosen to be used in the simulations because it is more stable, time efficient and still renders reasonable accurate results.

3.3 Implementation of the problem.

The problem of a whirling drillstring in a borehole as defined in chapter 2 has to be "translated" into a model which can be implemented in FLUENT. This implies constructing a geometry which describes the drillstring and the borehole wall, assigning boundary conditions to the drillstring and borehole wall in order to simulate the correct motions and constructing a grid so that the equations can be discretized and solved.

3.3.1 The geometry

The geometry for the model is rather straightforward (see figure 3.2)

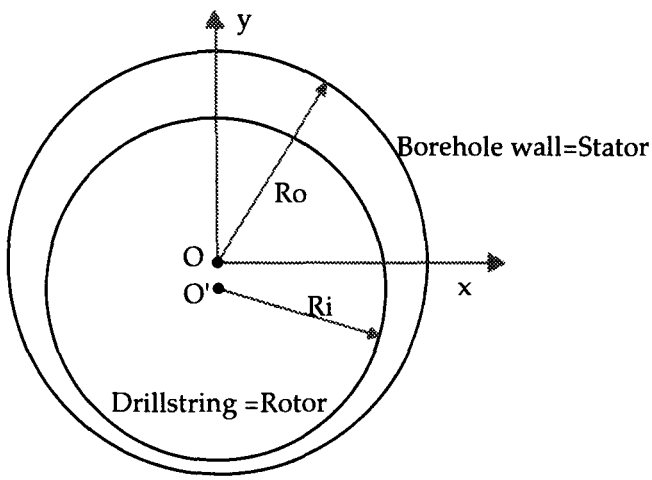

Figure 3.2: Problem geometry in FLUENT. O-O' is the displacement d of the rotor.

The outline of the geometry can be created in preBFC and has to be adjusted if a different eccentricity is considered. The displacement d of the rotor is always along the negative y-axis. The lift and drag force are thus positive in the negative y and x direction, respectively. The ratio of the inner and outer radius $\eta=R_i/R_o$ can also be adjusted.

3.3.2 The boundary conditions

In order to simulate the whirling motion in the geometry of figure 3.2, boundary conditions have to be implemented on the rotor and stator. The problem is simulated in a rotating reference frame because this leads to simple boundary conditions on both rotor and stator. Figure 3.3 shows the four different whirl motions (see section 2.2 Figure 2.3) in a reference frame rotating with angular velocity Ω.

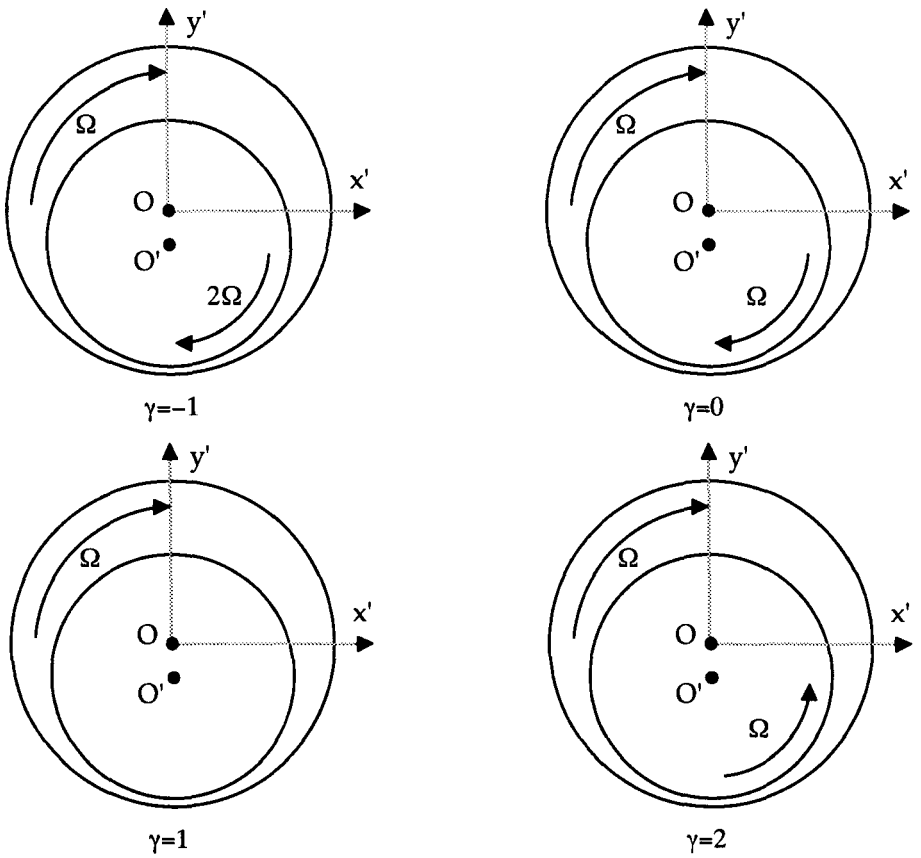

Figure 3.3: Four different whirl motions in the rotating reference frame. The rotor is down scaled for clarity.

For the case of backward whirl (γ=-1) the boundary conditions in the rotating frame will be explained. In the x,y frame γ=-1 is a rolling motion of the rotor along the stator wall. Consider now the rotating reference frame x',y'. This frame rotates with angular velocity Ω thus the motion of the rotor consist only of rotation around O'. The stator now rotates at an angular velocity Ω. The rotation velocity of the rotor in x',y' is twice the rotation velocity in x,y. This is due to the definition of the motion in x,y.

The advantage of considering the problem in a rotating reference frame is that the boundary conditions for the velocities are tangential to gridlines. This increases accuracy and decreases processing time. More details on grid and gridlines are discussed in the next section

3.3.3 The grid

In order to solve the governing partial differential equations numerically, approximations to the partial differentials need to be introduced. In finite volume methods such as those used in FLUENT, the partial differentials are reduced to algebraic expressions by integrating the governing equations over discrete subdomains. The algebraic equations are subsequently solved within the domain of interest. Therefore, a

set of grid lines must be specified within the domain in order to create these subdomains. The process of creating this grid system is called grid generation. The quality of the grid is of critical importance to numerical simulations. A poorly constructed grid can cause divergence of the solution, long processing time and even physically incorrect results. In this section we will step by step construct a high quality non-uniform grid by considering some desirable properties and requirements.

- Grid size

The grid size is a consideration of two factors: accuracy and computation time. A grid consisting of a large number of cells will result in an accurate solution but will take a long time to complete an iteration. For the problem under consideration it was decided to use a 90x10 cell grid. This has been proven to be sufficiently accurate with the advantage of a low computation time per time step.

- Uniform grid (90x10 cells).

A uniform grid of 90 cells along the rotor and stator wall is created by marking the rotor and stator circumference with 91 equi distant marks or nodes. The annular gap width is divided in 10 nodes. The node distribution can now be interpolated by preBFC to construct a uniform 90x10 grid. preBFC uses an algebraic 4-point (cubic) interpolation method. In the physical domain this will result in a grid as shown in figure 3.4 a This corresponds to a rectangular grid in the computational domain (figure 3.4.b). Cyclic boundary conditions have to be imposed on the curves AB and CD. The curves AC and BD represent the stator and rotor wall. The cells on these last two curves are wall type cell to which the boundary conditions will be assigned. The other cells are computational cells or live cells and are used as control volumes.

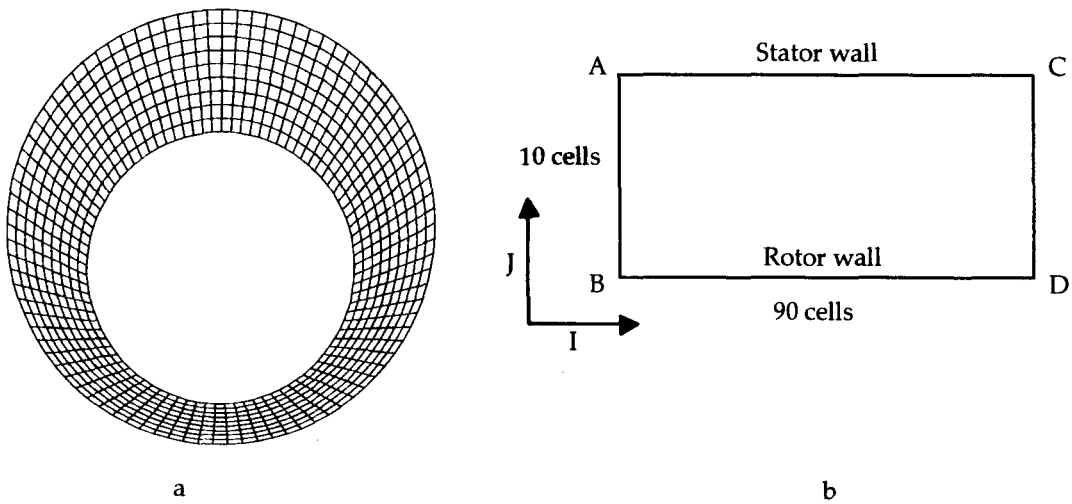

Figure 3.4: Uniform grid in physical and computational domain (ε=0.5)

-Grid spacing near walls

The basic flow in the annulus will be Couette type flow. The velocity gradients near a wall will be large compared to gradients in the middle of the annulus. Therefore the density of the grid lines should be sufficiently high near a wall to be able to adequately approximate the velocity gradients by the difference expression. For laminar Couette type flow between flat parallel plates separated by a height H it is recommended that:

$$\frac{\Delta n}{H} \leq 0.05 \tag{3.16}$$

where Δn is the distance between the wall and the first adjacent grid line. The density of the gridlines is now changed to meet these requirements.

-Grid skewness

Generated gridlines are often not orthogonal when using body fitted co-ordinates. While some degree of non-orthogonality is allowable, the computational grid should maintain grid intersection angles close to 90 degrees in order to simplify the discretized equations. The result is a more stable numerical solution procedure which converges more quickly Grid orthogonality can be achieved by redistributing the nodes on the stator wall and reinterpolating the grid.

-Cell aspect ratios

The cell aspect ratio is defined as;

$$a = \left(\frac{\Delta x_i}{\Delta x_j} \right)_{i \neq j} \tag{3.17}$$

where Δx_i, Δx_j are the cell dimensions in two coordinate directions. In general, this aspect ratio should not exceed 10 and should be closer to 1 in regions of complex flow. The stability of convergence can be affected by large cell aspect ratios. The aspect ratios can be controlled by the mapping of the nodes on the edges of the grid. A grid constructed for our simulations which satisfies the above mentioned requirements is shown in figure 3.5

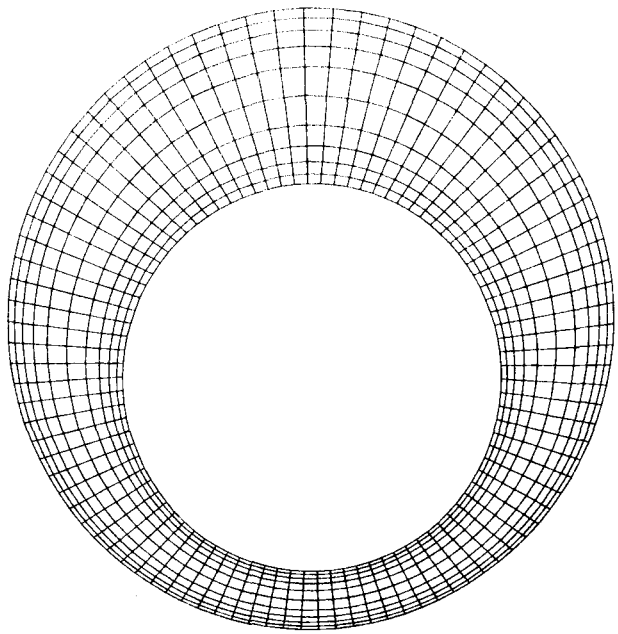

Figure 3.5: Non-uniform standard grid (90x10 cells) as used in simulations (ε=0.5)

3.4 The solution method

FLUENT uses a control volume based technique to solve the conservation equations for mass, momentum and turbulence quantities as described in section 3.3. This control volume technique consists of:

- division of domain into discrete control volumes using a general curvilinear grid as discussed in the previous section,

- integration of the governing equations (section 3.2) on the individual control volumes to construct the algebraic equations for the discrete unknowns (velocity, pressure, scalars),

- solution of the discretized equations.

The discretization of the differential equations, and the techniques used by FLUENT to solve them are described in this section.

3.4.1 The control volume technique

FLUENT is based on a control volume technique to convert the differential conservation equations to algebraic equations which can be solved numerically. This control volume technique consists of integrating the differential equations about each control volume, yielding a finite difference evaluation that conserves each quantity in a control volume. FLUENT defines the discrete control volumes using a non-staggered grid storage system. In this scheme, the same control volume is employed for integration of all the conservation equations and all variables are stored at the control volume cell centre. The integration of the differential equations can be illustrated most easily for a one dimensional equation set (see figure 3.6)

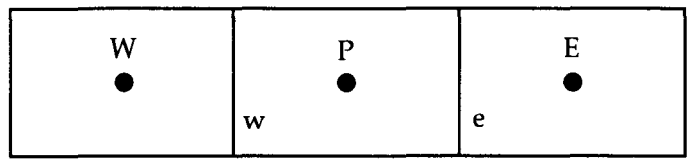

Figure 3.6: One dimensional control volume nomenclature used to illustrate volume integration

Consider first the one dimensional differential equations for continuity and momentum

$$\frac{\partial}{\partial x}(\rho u) = 0$$
$$\frac{\partial}{\partial x}(\rho u u) = -\frac{\partial p}{\partial x} + \frac{\partial}{\partial x}\left[\mu\left(\frac{\partial u}{\partial x}\right)\right] + F \tag{3.18}$$

Volume integration by employing the divergence theorem on the control volume of figure 3.6 thus yields for the continuity equation

$$J_e - J_w = 0, \quad \text{where} J = \rho u A \tag{3.19}$$

and for the momentum equation

$$J_e u_e - J_w u_w = -(p_e - p_w)A + \left[\frac{\mu_e}{\Delta x_e}(u_e - u_p) - \frac{\mu_w}{\Delta x_w}(u_p - u_w)\right]A + F\Delta V \tag{3.20}$$

These equations are algebraic equations which can be solved provided that the basic unknowns (u and p) are interpolated in a manner that relates their values at the control volume faces to the stored value at the control volume centres. The discretization procedures to perform this interpolation are discussed in the next section.

3.4.2 Discretization procedures

The interpolation to determine face values of the unknowns is accomplished via either the Power law, blended second order upwind/central difference or QUICK interpolation scheme. All schemes have been used and the difference in results was minimal for laminar flow. For turbulent flow however the higher order schemes were more accurate. Of these, the QUICK scheme was faster so this interpolation scheme was used in most simulations and is described below. A complete discussion can be found in [FLU 1994] and [LEO 1979].

The higher order QUICK scheme computes the face value of an unknown (e.g. ϕ_f) based on the value stored at the two adjacent cell centres (ϕ_P and ϕ_E) and on a third cell centre at an additional upstream point (e.g. ϕ_W). Using the nomenclature depicted in figure 3.7, the face value can be written as:

$$\phi_f = \theta\left[\frac{\Delta x_D}{\Delta x_C + \Delta x_D}\phi_C + \frac{\Delta x_C}{\Delta x_C + \Delta x_D}\phi_D\right] + (1-\theta)\left[\frac{\Delta x_U + 2\Delta x_C}{\Delta x_U + \Delta x_C}\phi_C - \frac{\Delta x_C}{\Delta x_U + \Delta x_C}\phi_U\right] \quad (3.21)$$

where ϕ_f is the face value, ϕ_D is the downstream value, ϕ_C is the centre cell value and ϕ_U is the upstream value

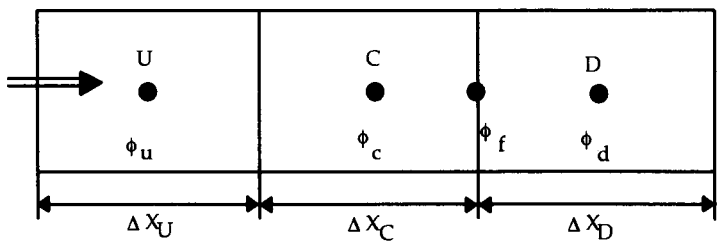

Figure 3.7: Central, downwind and upwind cell nomenclature employed in QUICK scheme

In equation 3.21 θ is chosen by FLUENT in a way which eliminates oscillation or overshoots.

3.4.3 SIMPLEC algorithm

The SIMPLEC (SIMPLE-Consistent) algorithm is a variant on the standard SIMPLE algorithm. The algorithms of the SIMPLE family are based on using a relationship between velocity and pressure corrections in order to recast the continuity equation in pressure correction terms. The SIMPLEC algorithm starts from the linearized discrete momentum equation (in 1D Cartesian form):

$$A_P u_P = \sum_{NB} A_{NB} u_{NB} + (p_w - p_e)A + S \quad (3.22)$$

where A_P and A_{NB} are the finite difference coefficients containing convection and diffusion terms, u_P and u_{NB} are the local velocity and neighbour velocity values and p_e and p_W are the face pressures acting across the control volume. Equation 3.22 is solved to obtain a guess for the velocity, u_P^* using the current guess for pressure, p^* as:

$$A_P u_P^* = \sum_{NB} A_{NB} u^*_{NB} + (p^*_w - p^*_e)A + S \quad (3.23)$$

The actual velocity and the pressure fields are related to these "guessed " values as:

$$u_P = u_P^* + u_P' \qquad p_P = p_P^* + p_P' \quad (3.24)$$

where u'_P and p'_e are the velocity and pressure corrections, respectively. Substitution of eq. 3.24 into 3.22 followed by subtraction of the current "guessed" momentum balance (eq. 3.23) yields a momentum balance in terms of the velocity and pressure corrections:

$$A_P u_P' = \sum_{NB} A_{NB} u'_{NB} + (p'_w - p'_e)A \tag{3.25}$$

Equation 3.25 is used to relate the velocity and pressure corrections, after subtraction of a new term, $\sum_{NB} A_{NB} u'_P$, from both the left and right hand sides:

$$\left(A_P - \sum_{NB} A_{NB}\right) u_P' = \sum_{NB} A_{NB}\left(u'_{NB} - u'_P\right) + (p'_w - p'_e)A \tag{3.26}$$

Next, the term involving the difference $(u'_{NB} - u'_P)$ is dropped under the argument that this term is small and will vanish at convergence when the corrections are zero. The resulting relationship between pressure and velocity corrections becomes:

$$u'_P = \frac{1}{A_P - \sum_{NB} A_{NB}} (p'_w - p'_e)A \tag{3.27}$$

Equations similar to eq. 3.27 are used to cast the continuity equation in terms of an equation for the pressure correction. The mass balance equation is first written in terms of the velocity u*+u':

$$(\rho A)_e (u^* + u')_e - (\rho A)_w (u^* + u')_w = 0 \tag{3.28}$$

Using equations similar to eq. 3.27, this continuity equation can be recast in terms of pressure correction, as:

$$\begin{aligned}(\rho A u^*)_e - (\rho A u^*)_w + (\rho A)_e \frac{1}{\left(A_P - \sum_{NB} A_{NB}\right)_e} (p'_P - p'_E) - \\ (\rho A)_w \frac{1}{\left(A_P - \sum_{NB} A_{NB}\right)_w} (p'_W - p'_P) = 0\end{aligned} \tag{3.29}$$

Equation 3.29 can now be solved for a correction to the pressure field which is then used to compute the velocity correction via 3.27. Finally, using eq. 3.24 the velocity and pressure corrections thus obtained are used to update the current velocity and pressure fields.

3.4.4 The iterative solution procedure

The SIMPLEC algorithm described above relates the velocity and pressure fields which satisfy the linearized momentum and continuity equation at a point. Because FLUENT does not solve the equations at all points simultaneously, and because the equations are coupled and non-linear, an iterative solution procedure is required with iterations continuing until all equations are satisfied at all points. Each iteration of FLUENT's solution procedure consists of the following steps:

1. The u_1 and u_2 momentum equations are solved in turn using the guessed pressure field p^*.

2. The pressure correction equation (mass balance) is solved to obtain the necessary corrections to the pressure field. Corresponding corrections to the velocity components are also made.

3. For turbulent flows, the k and ε equations are solved using the updated velocity field to obtain the distribution of the effective viscosity and/or Reynolds stresses.

4. Fluid properties are updated

These steps are continued until the error in each conservation equation within each volume and hence over the global domain has decreased to a required value. In the simulations the normalized residual value was 1.10^{-3}. The algebraic equation to be solved for any variable ϕ at point P may be written as:

$$A_P\phi_P = \sum_{NB} A_{NB}\phi_{NB} + S_\phi \qquad (3.30)$$

where the subscript NB denotes the neighbour values, the coefficients A_P and A_{NP} contain convection and diffusion coefficients and S_φ is the source of ϕ in the control volume surrounding point P. For each unknown, ϕ, an equation of this form must be solved at all points within the domain. This solution process is accomplished via a "line by line" solver in which the equations along a single line of cells are solved simultaneously. The procedure used in FLUENT is the line Gauss-Seidel method [FLU 1993] and is repeated for all lines in the domain so that ϕ is updated at all points P. There is some degree of freedom in this line by line solution procedure; the direction of the lines to be considered can be controlled and the number of times each line is visited in order to update a given variable within each global iteration loop. In the simulations a alternate sweep direction was used and the number of loops for pressure and velocity was 10 and 5, respectively.

This line by line solution method reduces local errors with relative ease. That is, the effect of the solution on one line is communicated to adjacent lines relatively quick. However the line-by-line solver is less effective at reducing "long wavelength errors" (errors which exist over a large number of control volumes. Multigrid acceleration of the solver provides a remedy for this weakness in the line solver by deriving "global" corrections which are based on a control volume balance over a large number of cells. Besides reducing long wavelength errors the multigrid procedure also speeds op the solution. [FLU 1993].

Chapter 4. The results

4.1 Introduction

A wide variety of simulations has been carried out to determine the influence of the four non-dimensional parameters ε, γ, η and Ta on the hydrodynamic force and the flow in the annulus. These simulations can be divided in to three categories: the concentric case, the eccentric laminar case and the eccentric turbulent case. The concentric case consists of simulations which were carried out for $\varepsilon=0$, $\eta=0.63$ and at Taylor numbers ranging from 13 up to 935. The results of this set will be given in section 4.2. The eccentric laminar case is a set of simulations which was carried out at $\Omega=0.008$ rad/s for varying ε, γ and η. The results of this set will be given in section 4.3. The final category of simulations is the eccentric turbulent case. This set of simulations was carried out at $\Omega=0.2$ rad/s for varying ε and γ. The results of this set will be given in section 4.4. A complete list of all the simulations can be found in Appendix 1.

Before we continue some important notes have to be made. In figure 4.1 a schematic recapitulation of the definition of various parameters is given. In this figure the annulus is divided into 4 regions which will be useful for the discussion in the remainder of this chapter.

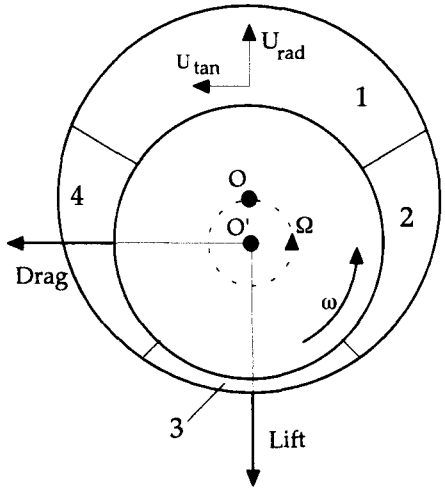

Figure 4.1: Definition of directions and nomenclature for the annulus regions.

Furthermore it has to be stressed that the streamfunction plots, which will be discussed in this chapter, are given relative to the rotating reference frame while the other plots (pressure distribution and turbulent kinetic energy) are also valid in an inertial reference frame. All the results will be discussed relative to the rotating reference frame unless explicitly stated otherwise. Due to practical reasons the colour plots, numbered C.1-C.15, are placed at the end of sections 4.3 and 4.4. Their scales will be briefly explained in these sections. A more detailed discussion is given in Appendix 2.

4.2 Concentric rotor

This set, consisting of four simulations, was carried out at different rotational velocities, which are given in table 4.1 along with their corresponding Taylor numbers. The flow in the annulus thus ranges from laminar to turbulent. The whirling velocity for this case is of course zero. The definition of the Taylor number is slightly different from the one for eccentric whirl (see table 2.2) but the same as used by Schlichting, so the results can be easily compared.

ω [rad/s]	$Ta_{con.} = \frac{\omega R_i C}{\nu}\sqrt{\frac{C}{R_i}}$
0.008	13
0.02	37
0.2	374
0.5	935

Table 4.1: Rotational velocities of the rotor and corresponding Taylor numbers
ν=1.002 10^{-6} m^2/s, R_i=0.0635 m and R_o=0.1016 m

We will now take a look at some flow features in the annulus like the stream function and the pressure distribution, followed by a discussion of the influence of the Taylor number on the torque.

4.2.1 Flow features in the annulus

A useful tool for studying fluid flow is the stream function ψ which can be defined for a 2D, steady, incompressible flow in cylindrical coordinates as:

$$u_r = \frac{1}{r}\frac{\partial \psi}{\partial \theta} \; ; \; u_\theta = -\frac{\partial \psi}{\partial r} \tag{4.1}$$

Thus a streamline (line of constant ψ) is a line for which the fluid velocity is everywhere tangential to the direction of that line. Figure C.1 shows the streamlines for Ta =37. The colour scale for streamfunction plots ranges from zero (red) to large

negative (blue). From the figure it is obvious that the flow in the annulus is a Couette type of flow. For this type of flow in an annulus between two concentric cylinders the flow velocity and pressure in the radial direction can be calculated analytically from mass and momentum conservation equations:

$$\frac{u_\theta^2}{r} = \frac{1}{\rho}\frac{\partial p}{\partial r} \tag{4.2}$$

$$0 = \mu \frac{d}{dr}\left[\frac{1}{r}\frac{d}{dr}\left(r u_\theta\right)\right] \tag{4.3}$$

This yields for the velocity:

$$u_\theta = Ar + \frac{B}{r} \tag{4.4}$$

with constants defined as:

$$A = -\frac{\omega R_i^2}{R_o^2 - R_i^2}, \quad B = \frac{\omega R_i^2 R_o^2}{R_o^2 - R_i^2} \tag{4.5}$$

In figure 4.2 a and b the analytical calculated velocity and pressure relative to the operating pressure for the case of Ta=37 are compared to the values in the simulations. Theory and simulations are in good agreement.

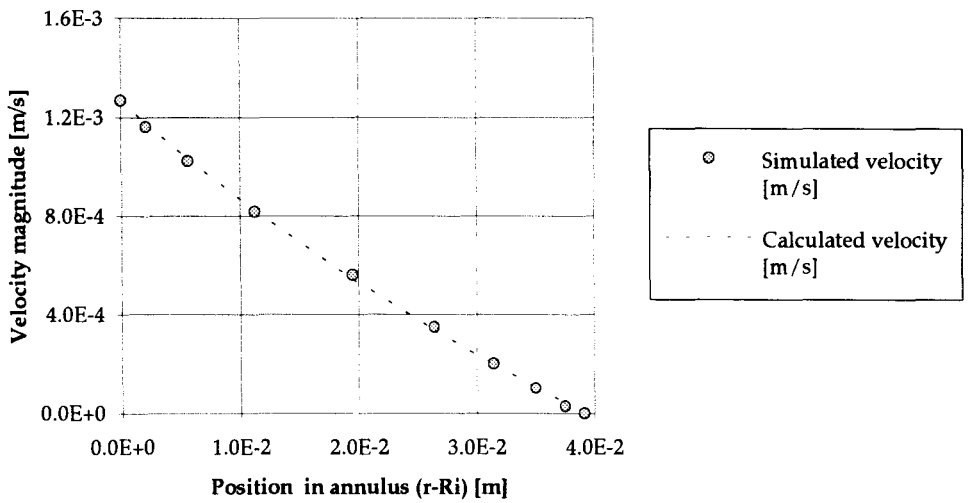

Figure 4.2.a: Velocity over a cross section of the annulus for Ta=37

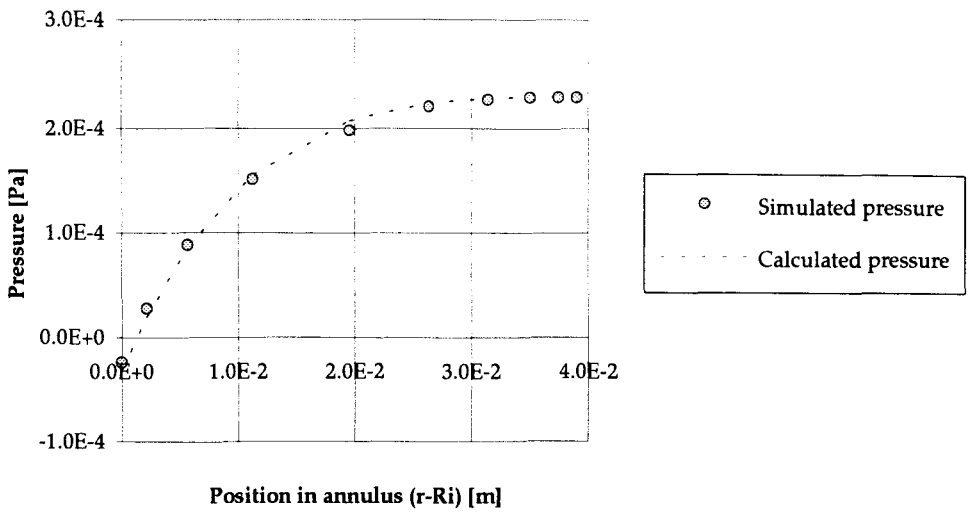

Figure 4.2.b: Pressure over a cross section of the annulus for Ta=37

4.2.2 Torque on rotor

An important and well studied property of flow between two concentric cylinders is the torque exerted by the fluid on the rotating cylinder. To get a validation and an idea of the accuracy of the method used in the simulations the torque on the rotor was calculated for the four Taylor numbers and compared with theoretical values as given in Schlichting's Boundary-Layer Theory [SCH 1979]. These theoretical values are supported by experiments. Figure 4.3 shows the torque coefficient C_M, as defined in section 2.3.2, as a function of the Taylor number.

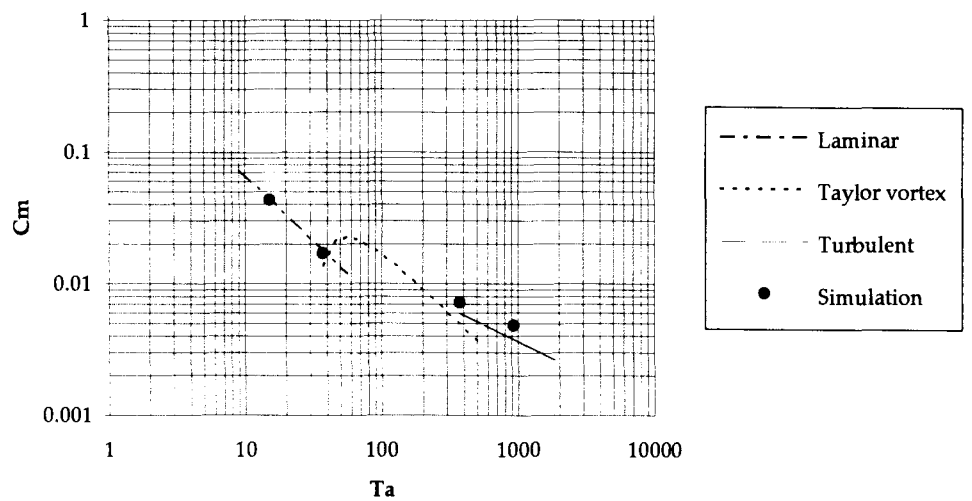

Figure 4.3 : Torque coefficient C_M as function of Ta.

The simulations are in good agreement with the theory for the laminar case. For the turbulent regime a certain offset from the theoretical values is found. This will be discussed in greater detail in section 5.4.1.

4.3 Eccentric whirling rotor; laminar case

All simulations in this category were carried out at a whirl velocity Ω=0.008 rad/s. The rotational velocity was varied between -0.008 rad/s and 0.016 rad/s yielding a γ ranging between -1 and 2. The eccentricity ε was varied between 0.1 and 0.9 while the ratio of the inner and outer radius, η, was either 0.63, 0.7 or 0.9. For these parameters the flow is in the laminar region thus the dominating force will be the viscous force. It should be mentioned that the characterisation of the flow by the Taylor number in a eccentric whirling situation is non-trivial. This will be discussed in detail in section 5.3. In the sections 4.3.1 through 4.3.3 the change in flow as a function of ε, γ and η is considered while in the sections 4.3.4 through 4.3.6 the influence of these parameters on the rotor surface pressure is studied. All colour plots are given at the end of section 4.3.

4.3.1 Flow in the annulus as function of ε

To obtain a clear understanding of the change of flow with increasing eccentricity we will consider stream line patterns, keeping in mind that these represent the flow in the rotating reference frame. First consider backward whirl, γ=-1 for η=0.63. Figure C.2. shows the stream function for three different eccentricities. For low eccentricity (ε=0.1) the flow in the annulus resembles Couette flow (compare to fig. C.1) which is as expected since there is only a small change in the geometry with respect to the concentric case. If the eccentricity is increased to 0.5 the distribution of the streamlines in region 1 becomes less dense which implies a lower u_θ. The opposite occurs in region 3 resulting in a higher U_θ. This is caused by conservation of mass flux. Increasing the eccentricity further to 0.9 yields a totally different pattern for the streamlines. Two recirculation areas can clearly be distinguished in region 1. The direction of the circulation in the top area is opposite to that of the bottom area. This result can be compared to results discussed by Ottino [OTT 1989] (see figure C.3). In the example studied by Ottino η=0.33, ε=0.8 and γ=-3 so the stream function will differ in some details but the general behaviour is identical to our case.

4.3.2 *Flow in annulus as function of* γ

To determine the influence of γ on the flow in the annulus we will consider the case for ε=0.9 and η=0.63. At these values the influence on the two recirculation areas can be examined. Simulations were done for γ=-1,0,1,2. Figure C.4 shows the resulting stream functions. It can be seen that the bottom recirculation area (the one close to the rotor) does not exist for values of $\gamma \geq 1$. Consider the case of γ=2; the stator rotates clockwise at Ω, the rotor rotates counter clockwise at 2Ω. The annulus width in region 3 is so small that it will block the flow almost entirely. Thus a recirculation area now occurs in region 1 with the direction of flow determined by the direction of rotation of the walls. For γ=1 the flow is similar. If the rotor is static (γ=0) or rotates in a clockwise direction (γ=-1) the no slip condition on the rotor wall will create a shear flow between the fluid near the rotor wall and the flow in the recirculation area. This induces the second recirculation area near the rotor wall.

4.3.3 *Flow in annulus as function of* η

For three values of eccentricity (ε=0.1,0.5,0.9) and two values of γ (-1 and 1) the ratio of the radii, η, was increased from 0.63 to 0.7 and 0.9. The formation of the recirculation areas will be suppressed and actually disappear for high η. These effects have been observed in studies on journal bearings. For η=0.9 the simulation at ε=0.9 has not been carried out because a grid with different characteristics is required. This is due to the extremely large pressure gradients in both radial and tangential direction. Such a grid has not been constructed. To show stream function plots for ε =0.5 is of no interest since recirculation areas have not formed yet. The influence of η on the forces and torque can however be deducted from our limited set of numerical experiments. This will be discussed in section 4.3.6.

4.3.4 *Pressure on rotor as function of* ε

Due to the fluid in the annulus shear and normal forces are exerted on the rotor which result in a torque and a lift and drag force. The shear forces determine the torque on the rotor while the normal forces are the dominating factor for the lift and drag force. The normal forces result from the pressure distribution on the rotor. In the following sections the pressure relative to the operating pressure is considered. Following the same method as for the stream function we will first take a look at the change in pressure as function of the eccentricity at constant η and γ, followed by changing γ while ε and η are constant and finally studying the influence of η by holding γ and ε constant. At the end of section 4.3.6 the plots for lift, drag and torque as function of these three parameters are given.

Consider now the case of γ=-1 (backward whirl) for η=0.63 and Ω=0.008 rad/s. Figure C.5 shows the pressure distribution in the annulus for eccentricity ε=0.5. In all pressure distribution plots red represents high pressure regions and blue low pressure regions. The scales for the plots are relative (see also appendix 2). It is evident that the pressure increases on a line radially outward from the rotor to the stator. This is due to the centrifugal force caused by the rotation of the flow which

tends to push the fluid against the stator. For examining the lift and drag forces we do not need the pressure in the entire annulus just the pressure on the rotor wall. This is given in figure C.6 for η=0.63, γ=-1 Ta=13 and ε=0,0.1,0.5,0.9. In all these pressure distribution plots the value of the pressure is represented by the shape and colour of the contour. For ε=0 the pressure distribution on the rotor is of course uniform. Increasing the eccentricity to 0.1 results in a slightly higher pressure in region 1 and a low pressure in region 3. This pressure distribution can be explained by considering the rotor and stator motion in the rotating reference frame. Both the stator and rotor motion (for γ=-1) induce a clockwise flow which results in a pressure build up in the region where the annulus starts to narrow. The low pressure region occurs also as consequence of these motions. If the eccentricity is increased to 0.5 the same mechanism for the pressure build up is present but the build up will be more intense now since the channel becomes narrower. For ε=0.9 eventually the pressure distribution is of the same general shape as a lubrication profile (see figure C.7). In fact we are now dealing with a bad constructed journal bearing with a time dependent load [SHA 1949], the difference being that for a journal bearing η is almost unity while in our case η~0.7.

The resulting lift an drag forces are dominated by this pressure distribution. The influence of the shear forces on lift and drag is at least a factor 3 smaller. Considering the lift force we can see that it will be positive for small eccentricities and change to a large negative force for high eccentricities. The drag force is always positive and increases with eccentricity.

4.3.5 Pressure on rotor as function of γ

Let us consider now ε=0.5 for the same values of η, and Ω as above but for γ=-1 ,0,1,2. Figure C.8 shows the pressure on the rotor for this case. An increase in γ results in an increase of pressure in the high pressure region and a shift towards the part of the annulus were the gap is narrower (region 3). In the low pressure region the opposite happens (decrease of pressure and shift to region 1). This can again be explained by examining the rotor and stator motion. The stator motion induces a counter clockwise flow, yielding a pressure build up in region 2. This holds for all values of γ. For γ=-1 the rotation of the rotor will force fluid close to the rotor to flow in a clockwise direction thus adding to the pressure build up. For a value of γ=2 however the counter clockwise rotor motion will induce high pressure in region 4. Combined with the "stator effect" this results in the pressure distribution as seen in figure C.8. The pressure distribution for γ=0 or 1 can be explained analogous.

As a result the lift force changes from positive for γ=-1 to negative for γ=2 at this given eccentricity and rotational velocity. The drag forces decreases but remains positive.

4.3.6. Pressure on the rotor as function of η

The resulting effect of an increase in η on the pressure distribution is reasonable simple. Figure C.9 shows the pressure distribution in the entire annulus for η=0.63, 0.7, 0.9 at a constant ε and γ. An increase in η results in a slight shift of the location of the high and low pressure regions and "intensifies" the pressure. This implies that with an increase in η the drag and lift forces increase but do not change in direction which is a result well known from lubrication theories.

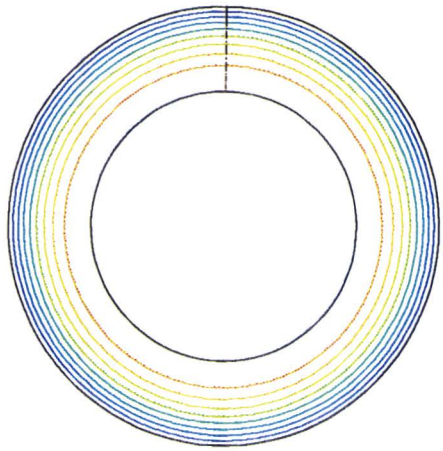

Figure C.1: Stream function in concentric annulus for η=0.63 Ta=37.

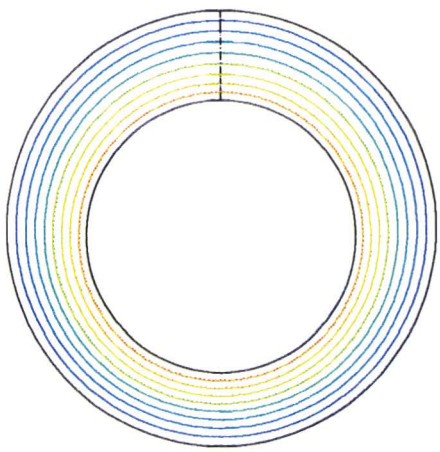

Eccentricity = 0.1

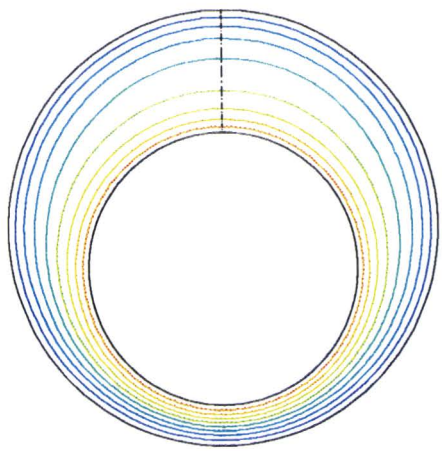

Eccentricity = 0.5

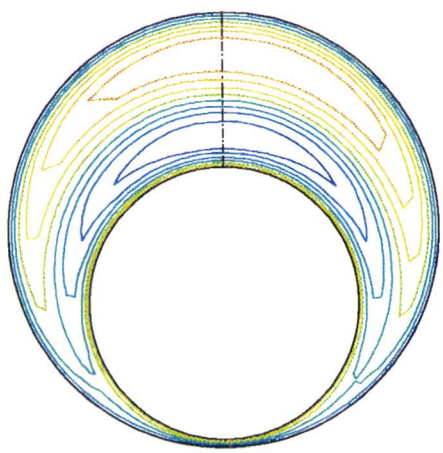

Eccentricity = 0.9

Figure C.2: Simulated stream function for different eccentricities. (γ=-1, η=0.63, Ta 13)

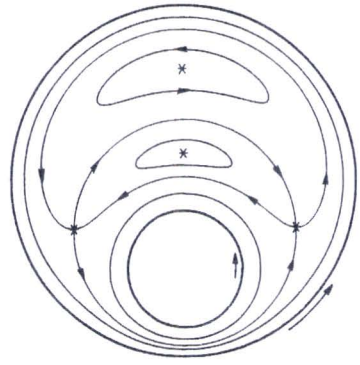

Figure C.3: Stream function as given by Ottino (γ=-3, ε=0.8,η=0.33 and Ta<1).

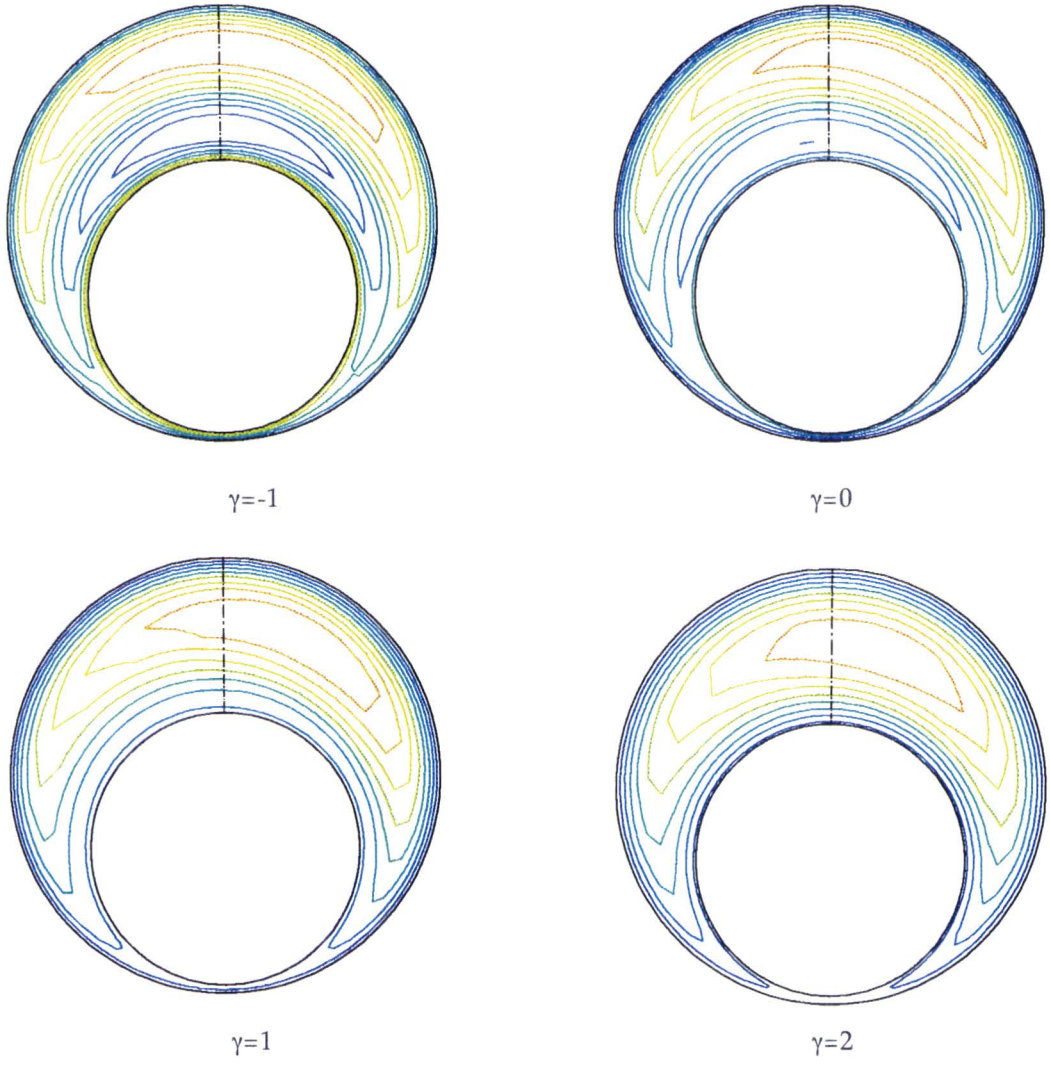

Figure C.4: Stream function for different γ values (ε=0.9, η=0.63, Ω=0.008 rad/s)

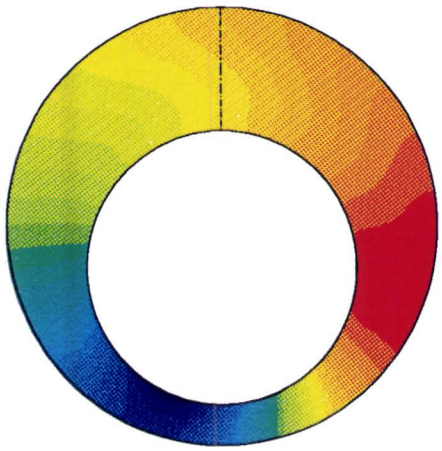

Figure C.5: Pressure in annulus (η=0.63, γ=-1, ε=0.5, Ta=13)

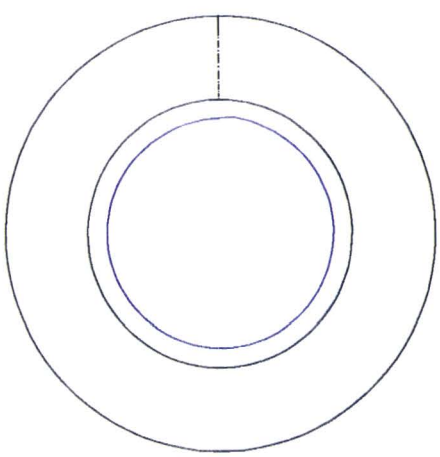

Concentric

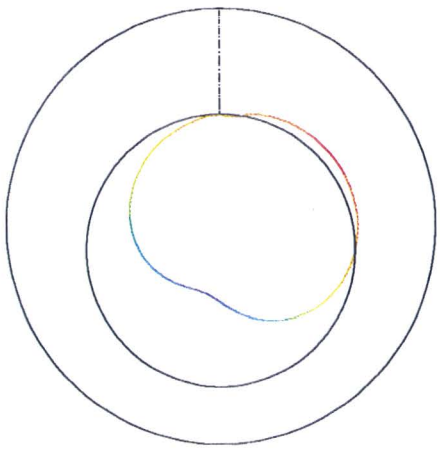

Eccentricity=0.1

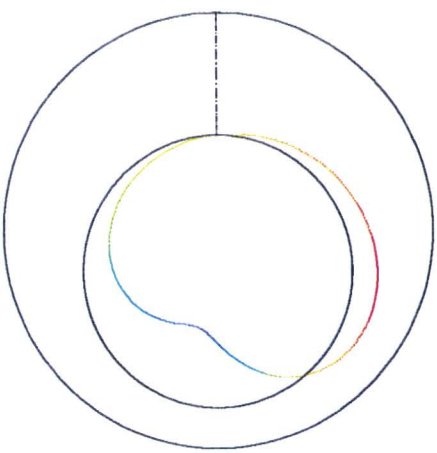

Eccentricity=0.5

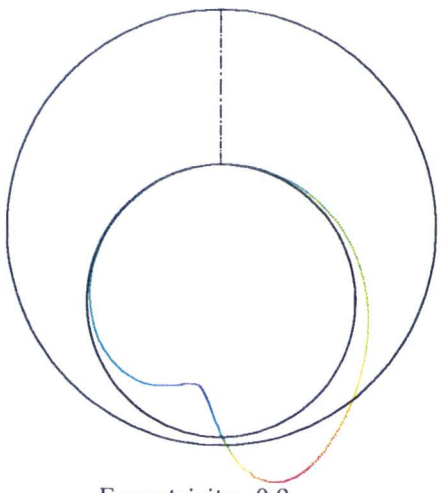

Eccentricity=0.9

Figure C.6: Pressure on rotor for different eccentricities (η=0.63, γ=-1, Ta=13)

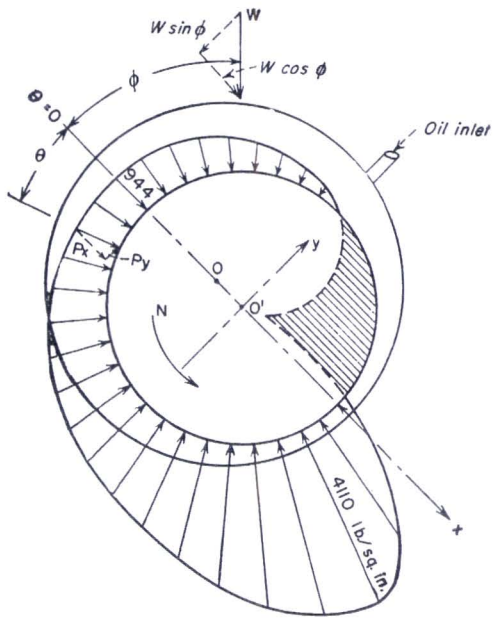

Figure C.7: Pressure on a journal bearing (without whirl) η=0.99 [SHA 1949]

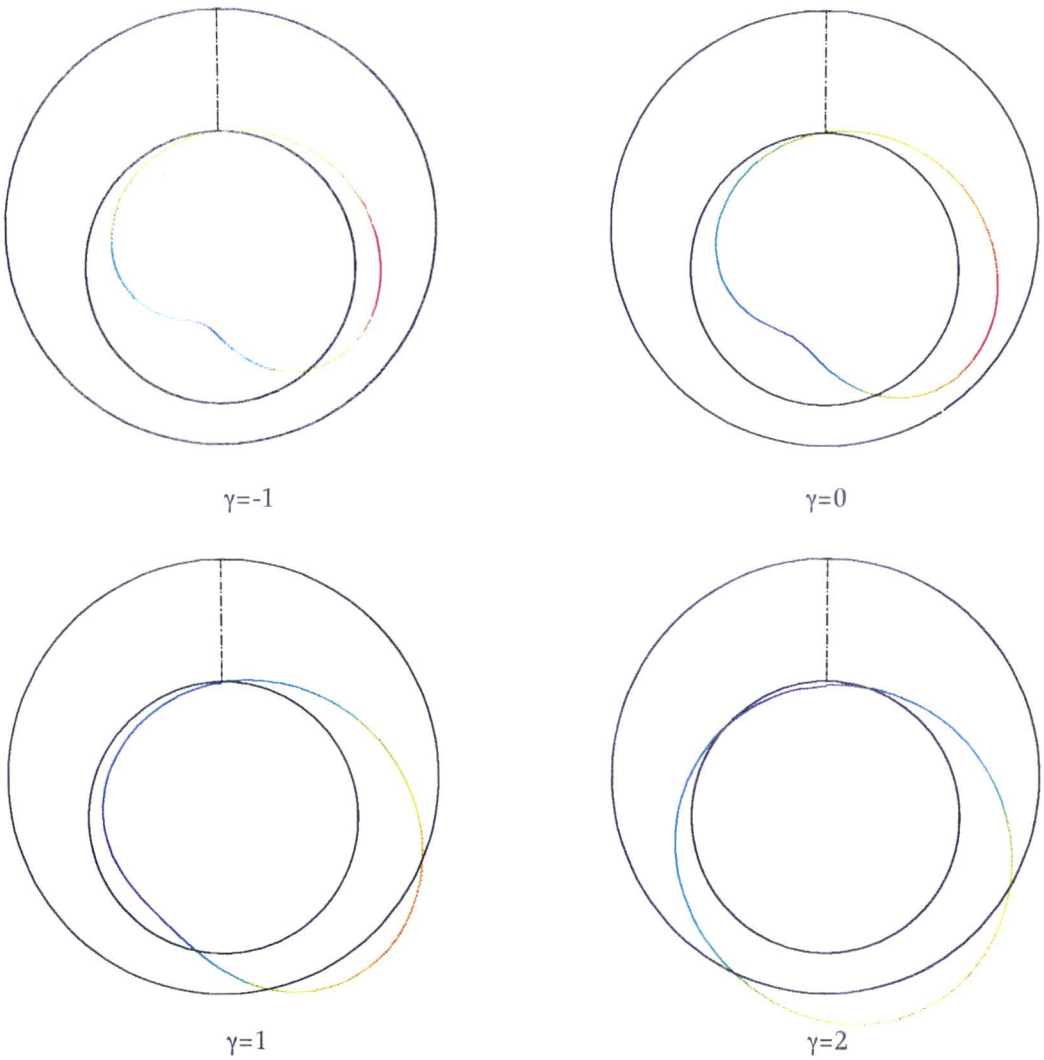

Figure C.8: Pressure on rotor for different γ values (ε=0.5, η=0.63, Ω=0.008 rad/s)

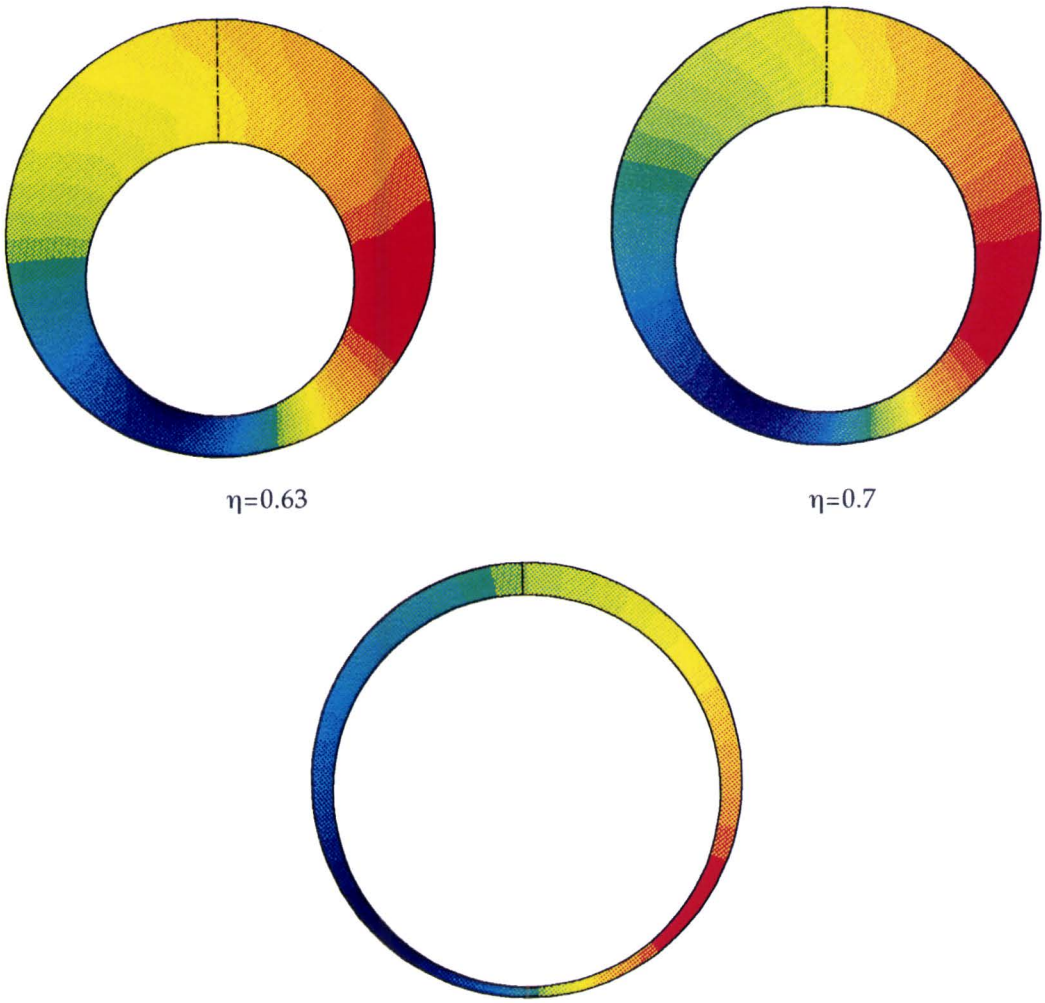

Figure C.9: Pressure in annulus with increasing η (ε=0.5, γ=-1, Ω=0.008 rad / s)

4.4 Eccentric whirling rotor; turbulent case

The simulations in this category are conducted in the same way as for the laminar case. The parameter η was now held constant at 0.63 in all simulations. The value of Ω was increased to 0.2 rad/s (Ta=374). The flow in the annulus will thus be mainly turbulent which implies that the inertia forces will be dominating. The turbulent flow was simulated using the k-ε turbulence model as described in section 3.2. Because of the similarity with the set-up of the simulations in the laminar case we will treat the turbulent case in the same way. First we will take a look at the influence of ε and γ on the flow in the annulus in sections 4.4.1 and 4.4.2. We will do this by studying the stream function and by studying the distribution of the turbulent kinetic energy (TKE) in the annulus. We then proceed by studying the influence of ε and γ on the pressure in the annulus in sections 4.4.3 and 4.4.4 The colour plots are given at the end of section 4.4.

4.4.1 Flow in annulus as function of ε

As mentioned above we will again study the streamfunction to get a good understanding of the flow features in the annulus. In addition to this we will also pay attention to the TKE distribution which is helpful in examining turbulent flow. The TKE plots are also used in the discussion of the Taylor number (section 5.3).

We will start by considering the backward whirl motion γ=-1. Figure C.10 shows the stream function for three different eccentricities ε=0.1,0.5,0.9. Although the flow is now dominated by inertia forces the difference with the laminar stream function patterns is minimal, the main difference being a shift in the position of the recirculation areas. Figure C.11 shows the distribution of turbulent kinetic energy (TKE) in the flow for the same parameters as figure C.10. In TKE plots a red colour corresponds to a region of high TKE where blue corresponds to a region of minimal or zero TKE. The scale is relative as is the case for all colour plots (see appendix 2). The TKE decreases for increasing eccentricity which implies a stabilizing influence of the eccentricity on the flow. This effect is discussed in detail in section 5.3.

4.4.2 Flow in annulus as function of γ

At a constant eccentricity ε=0.5 the value of γ is varied between -1 and 2 to examine the influence of γ on the flow. The stream functions for this case are depicted in figure C.12. The eccentricity ε=0.5 was chosen in order to study the creation of the first recirculation area. For increasing values of γ the recirculation area becomes more pronounced which can be explained as follows; flow velocities decrease in region 1 because of conservation of mass flux. For γ=2 the rotor and stator rotate in opposite directions (in the rotating reference frame). The resulting shear flow causes the flow velocity in the middle of region 1 to decrease further. Around this patch of "static" fluid the flow direction is determined by the rotation direction of the rotor and stator resulting in a recirculation area. This also explains why for γ=-1 no recirculation area will be present.

4.4.3 Pressure on rotor as function of ε

In order to examine the behaviour of the forces on the rotor we will again study the pressure in the annulus and on the rotor as a function of γ and ε. We will consider the influence of ε at a constant γ and then, holding ε constant, study the influence of γ. First we will take a look at a plot of the pressure in the entire annulus (Figure C.13). The obvious difference with the laminar case is a shift in the position of the high pressure region (compare to Figure C.5) which will be explained below. The force on the rotor is calculated from the pressure distribution on the rotor surface which is given for different eccentricities at γ=-1 in figure C.14. The pressure distribution for the concentric case will be uniform which is trivial. The pressure distribution for the non-concentric cases can be explained by utilising Bernoulli's equation. It has to be stressed that this approximation is not used in the calculation of the hydrodynamic force by FLUENT. It is merely discussed here to provide an insight in the flow mechanisms. Bernoulli's equation states that for inviscid, incompressible flow in a 2D horizontal plane;

$$\frac{1}{2}\rho V^2 + p = \text{constant along stream line} \tag{4.6}$$

where V is the velocity and p the pressure. The essence of this equation can be stated as: low velocity $\Leftrightarrow$ high pressure, high velocity $\Leftrightarrow$ low pressure. This equation is valid for the flow in the annulus if viscosity effects can be neglected which is more or less true if we look at the main flow region and stay away from the boundary layers. Consider now ε =0.1. From conservation of mass flux it follows that the flow velocity will be low for a wide annulus and high for a narrow annulus. By using Bernoulli's equation this yields that the pressure will be high for a wide flow region and low for a narrow flow region which is exactly what can be seen in figure C.14 As the eccentricity increases Bernoulli's equation no longer applies because the flow velocities decrease under the influence of the creation of recirculation areas. For these lower velocities the viscous forces increase. Thus the flow can no longer be considered inviscid. The validity of Bernoulli's equation is also influenced by γ since this parameter also determines the flow velocity (see section 4.4.4). For high eccentricities (ε=0.9) the rotor stator set-up starts behaving as poorly constructed journal bearing as explained in 4.3.4.

The resulting lift force will thus be positive for small eccentricities and change to a large negative force for large eccentricities. The drag force will grow steadily with eccentricity.

4.4.4 Pressure on rotor as function of γ

We will now consider the influence of γ for ε=0.5. The plots of the pressure on the rotor are given in figure C.15 Analogous to the previous section the Bernoulli equation can again be used to provide some insight in the flow. It was also already mentioned that the validity of Bernoulli's approximation is limited by both ε and γ. From figure C.15 it is plausible that for γ <1 the flow can be explained by Bernoulli's equation. For $\gamma \geq 1$ however the pressure distribution is different from the one predicted by Bernoulli. This is again caused by the generation of recirculation areas as explained in the previous section (see also Figure C.12). When these areas occur

the flow becomes viscid again. Thus the pressure on the rotor can be explained analogous to the laminar case.

For the forces this implies that the lift will change from positive for γ=-1 to negative for γ=2 while the drag will decrease but remain positive.

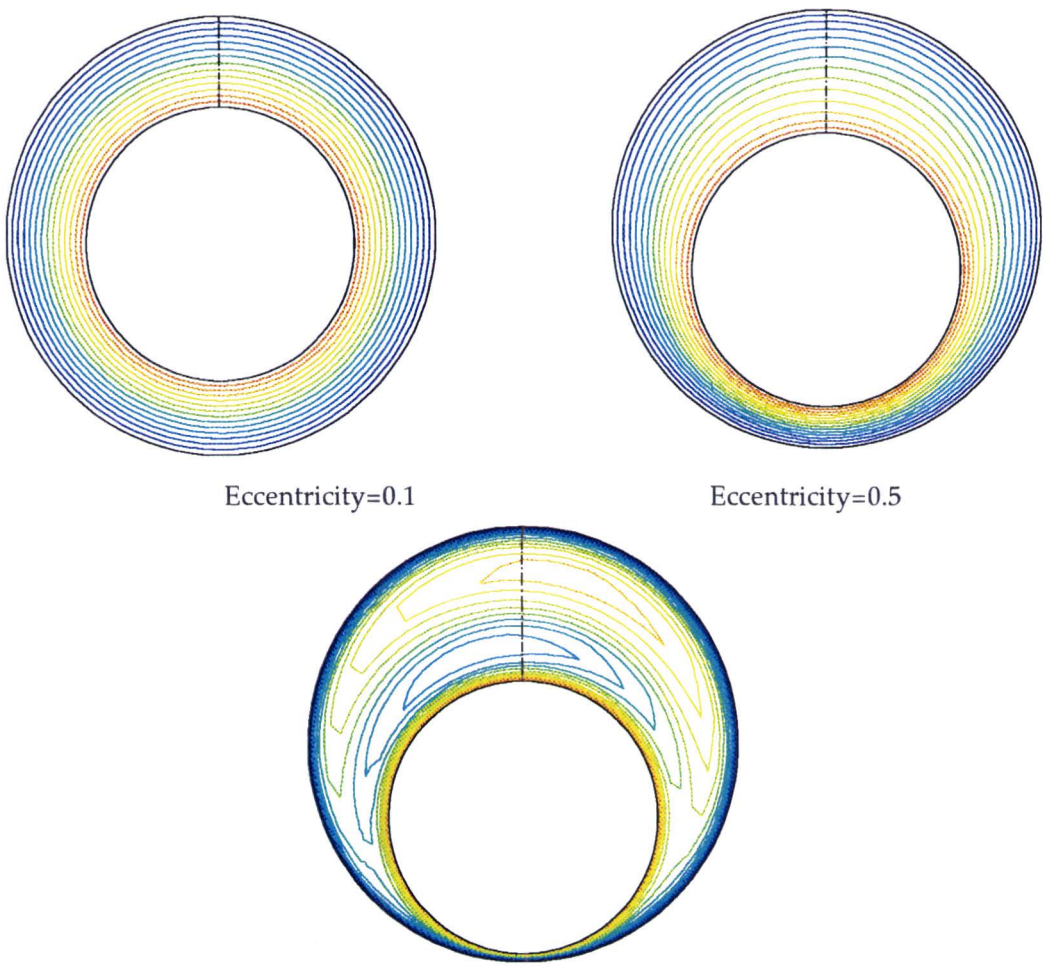

Figure C.10: Simulated stream funtions for different eccentricities (γ=-1, η=0.63 Ta=374)

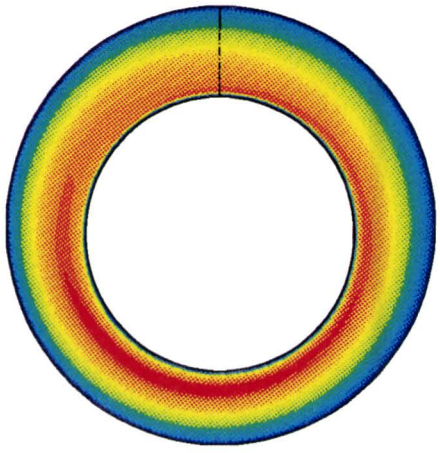

Eccentricity=0.1

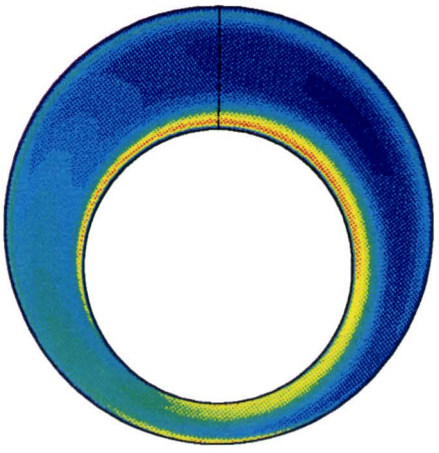

Eccentricity=0.5

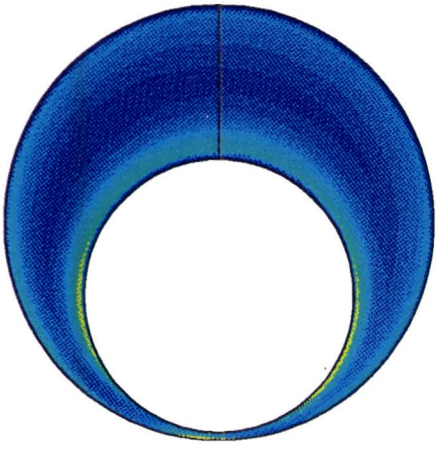

Eccentricity=0.9

Figure C.11: Simulated turbulent kinetic energy distribution for different eccentricities. (γ=-1,η=0.63, Ta=374)

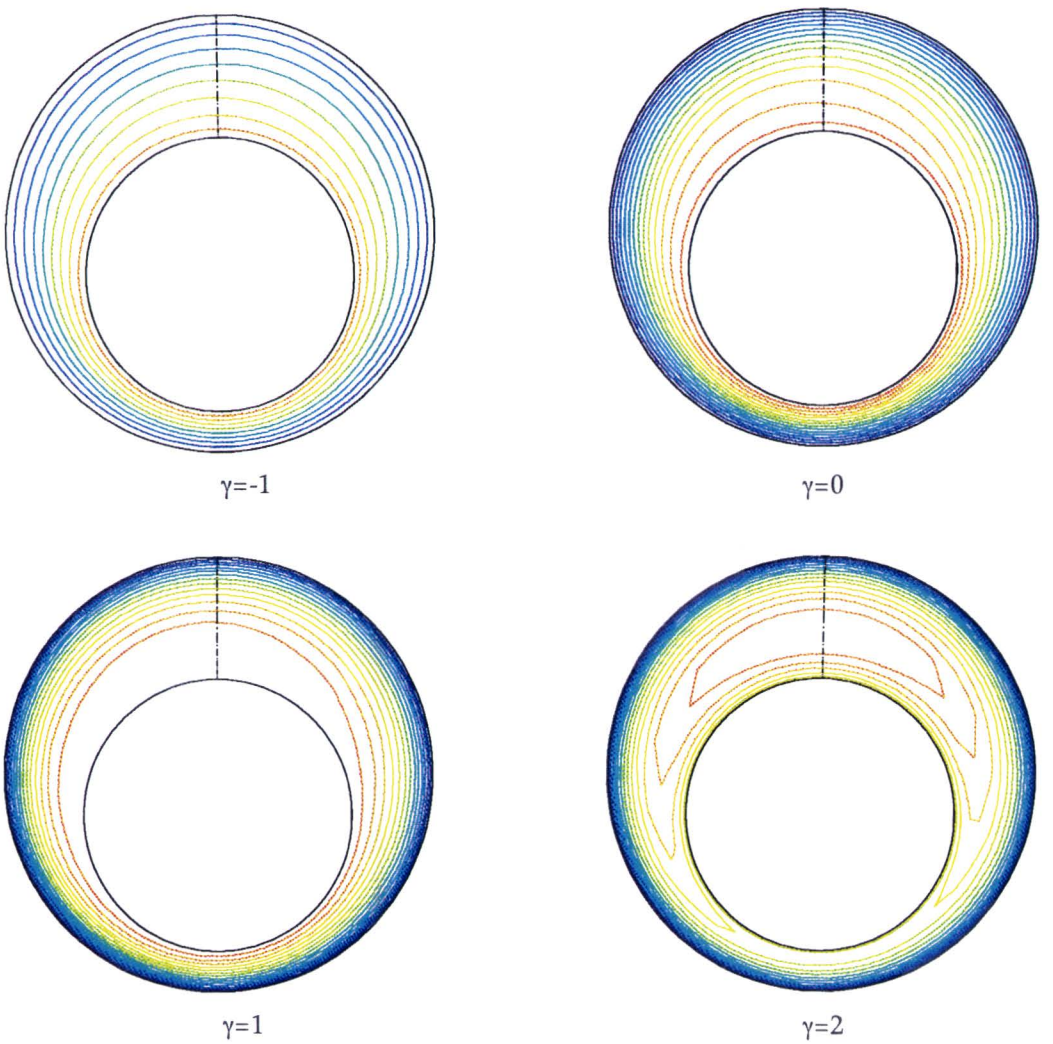

Figure C.12: Simulated stream function as a funtion of γ. (ε=0.5,η=0.63, Ω=0.2 rad/s)

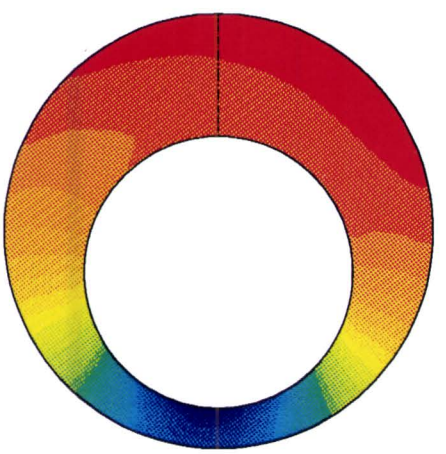

Figure C.13: Pressure in annulus (η=0.63, γ=-1, ε=0.5, Ta =374)

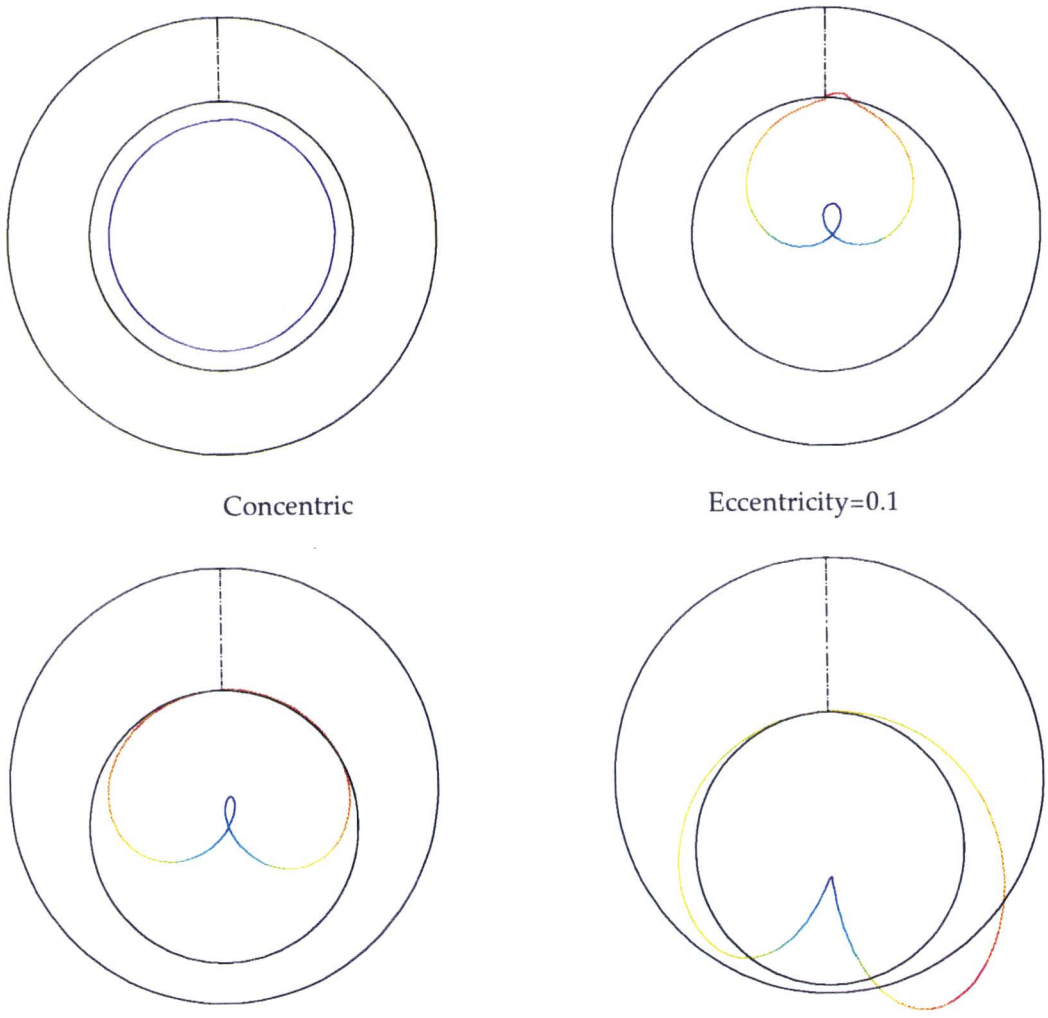

Figure C.14: Pressure on rotor for different eccentricities (η=0.63,γ=-1,Ta =374)

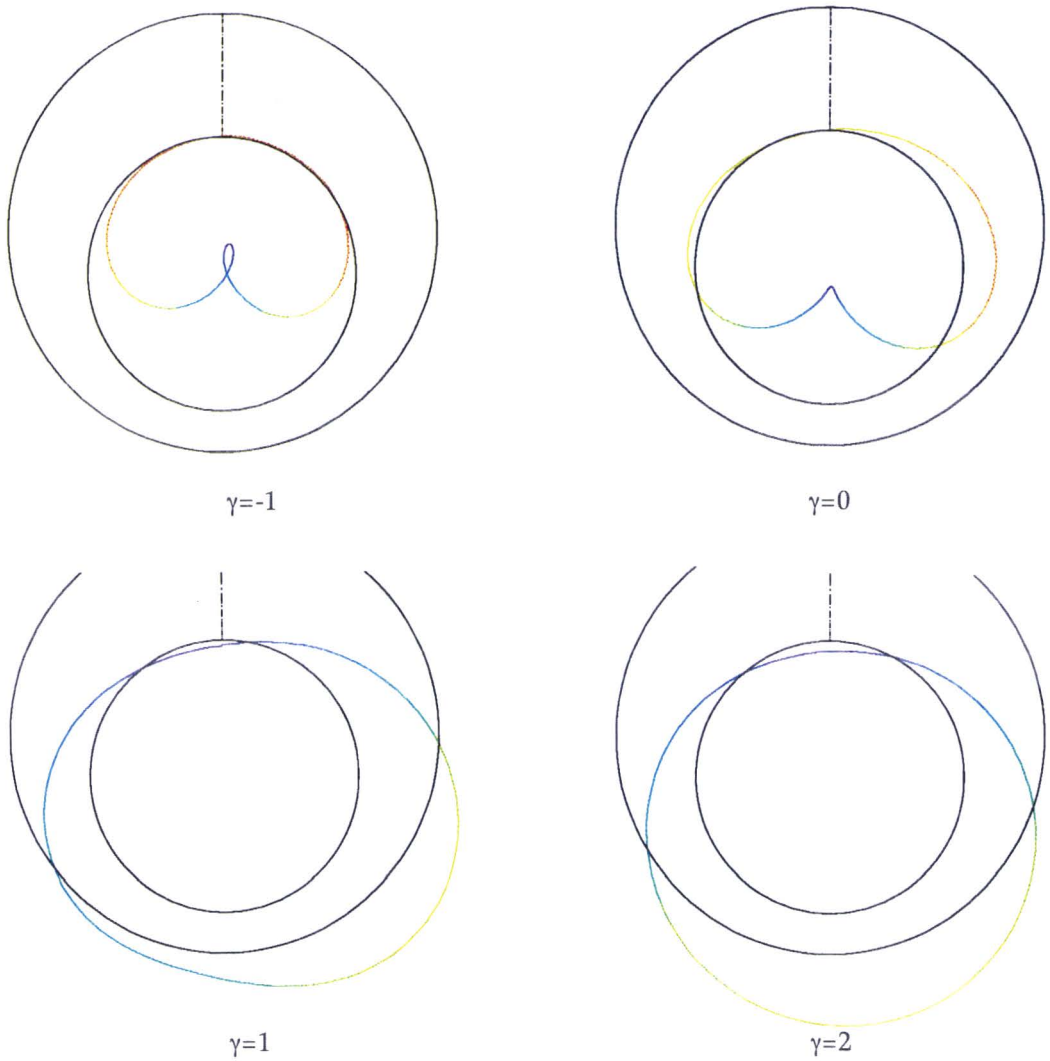

Figure C.15: Pressure on rotor as function of γ. (ε=0.5,η=0.63, Ta=374)

Chapter 5. Discussion

5.1 Introduction

In this chapter some key issues about the simulations will be thoroughly reviewed and discussed. The use of the Taylor numbers is discussed in section 5.3. We will start, in section 5.2, with a check of some basic requirements of the method like grid independence and the use of non-dimensional parameters and scaling factors. A complete discussion of the resulting hydrodynamic force and torque on the rotor is included in the confidential version of this report.

5.2 Basic check of method

Some basic features of the method have to be checked before the results can be considered of any significance. First of all the results of any numerical method have to be independent of the grid size. If the grid is refined enough to capture the flow features of interest further refinement should not alter the results significantly. Another issue that has to be checked is whether the problem is correctly characterized by the set of non-dimensional parameters and scaling factors.

5.2.1 Grid independence

The grid independence can be checked by running the same simulation for different grid sizes and comparing their results. This check has been performed at three different eccentricities, ε=0.2,0.5,0.9 and η=0.63 for γ=0 and γ=2 in both the laminar and turbulent case . The results were assumed to be valid for the complete set. The grids used in the test are listed in table 5.1.

Grid	number of cells	represented in plots by
Standard grid	90x10	○
half-standard grid (laminar)	45x5	▲
half-standard grid (turbulent)	45x10	▲
double-standard grid	180x20	◆

Table 5.1: List of grids used in grid independence tests.

The half-standard grid used in the turbulent simulations still consists of 10 cells across the annulus width which was necessary in order to fulfil the requirements made on the grid in the boundary layers.

In the laminar case the difference between the results decreases from 30% between the half-standard and standard grid to 5% between the standard and double-standard grid. In the turbulent case these values are 32% and 15%, respectively, implying no convergence to a grid independent solution. This is due to the values for ε=0.9. For this eccentricity the quality of the grid is less due to large aspect ratios and cell skewness. If lower eccentricities are considered the difference between the grids is 32% and 7% which is satisfactory. From this we may conclude that the change in results reduces sufficiently in order to consider the method reasonably grid independent.

5.2.2 Non-dimensional parameters and scaling factors

Buckingham's pi theorem, as mentioned in section 2.3.2, yields that the problem considered here is characterised by four non-dimensional parameters. Two flow problems can be considered identical if the set of non-dimensional parameters which describes them have the same values. This provides us with a way to check the relation between the chosen non-dimensional parameters and the scaling factors. Three simulations were carried out in which the dimensional parameters were changed but the non-dimensional parameters were identical. If the non-dimensional parameters and scaling factors characterise the flow correctly the results for C_L and C_D will be identical. This is the case as can be seen from table 5.2.

	R_i [m]	R_o [m]	d [m]	ω [rad/s]	Ω [rad/s]	ρ [kg/m^3]	μ [Pa s]	C_L	C_D
1	0.0635	0.1016	0.0191	0	0.008	998	0.001	3.90	14.6
2	0.0635	0.1016	0.0191	0	0.008	**1996**	**0.002**	3.90	13.8
3	**0.127**	**0.2032**	**0.0382**	0	**0.004**	**499**	0.001	3.92	15.2

Table 5.2: Dimensional parameters for three different simulations and the resulting lift and drag coefficients.(γ=0, η=0.63, ε=0.5, Ta=0)

5.3 Taylor number

Up until now we have used a Taylor number for eccentric flow defined as:

$$Ta_{glob.} = \frac{\omega R_i (R_o - R_i)}{\nu} \sqrt{2\frac{(R_o - R_i)}{R_o + R_i}} \qquad (5.1)$$

This Taylor number is a global number and is commonly used in articles about whirling flow [FRI 1970],[BRE 1976]. It is based on the definition of the Taylor number as used for concentric cylinders. Although it has been proven to be very

useful for the concentric case, there are reasons to doubt its validity for the case of an eccentric whirling cylinder.

First of all only the rotational velocity is accounted for thus neglecting the whirling velocity. Furthermore no eccentricity effects are taken into account which can be seen by considering the transition of laminar flow into Taylor vortex flow. Using the definition (eq. 5.1) the critical number is independent of the eccentricity. This is however incorrect as can be seen from experimental values of $Ta_{crit.}$. in figure 5.3.

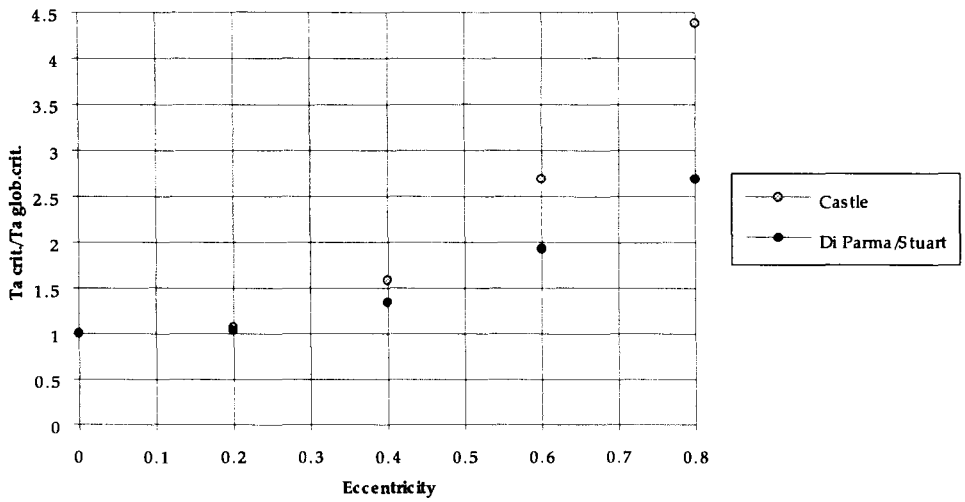

Figure 5.3: Experimental values for the critical Taylor number as function of the ε for an eccentric rotor (γ=0, η≈0.7).

From the experimental data it is evident that the eccentricity has a stabilizing effect on the flow. This stabilizing effect has also been found in the numerical experiments (see section 4.4). A different approach to a Taylor number is based on considering the flow locally at any section of the annulus [URB 1972]. For this purpose a local Taylor number is introduced:

$$Ta_{loc.} = \frac{U_{loc.}}{\nu}\sqrt{2\frac{C_{loc.}^{\ 3}}{R_o + R_i}} \tag{5.2}$$

where $C_{loc.}$ is the local annulus thickness and $U_{loc.}$ is the local velocity of the rotor in the inertial reference frame as calculated from eq. 5.3 (see also figure 5.4):

$$\begin{aligned} U_{loc.} &= \sqrt{\left(\omega R_i + \Omega x\cos(\theta-\phi)\right)^2 + \left(\Omega x\sin(\theta-\phi)\right)^2} \\ C_{loc.} &= \sqrt{R_o^2 - \left(x\sin(\theta-\phi)\right)^2} - x\cos(\theta-\phi) \end{aligned} \tag{5.3}$$

where

$$\theta = Arc\tan\left(\frac{\sin\phi}{\cos\phi - \frac{d}{R_i}}\right) \tag{5.4}$$

and

$$x = \sqrt{\left(R_i \sin\phi\right)^2 + \left(R_i \cos\phi - d\right)^2} \tag{5.5}$$

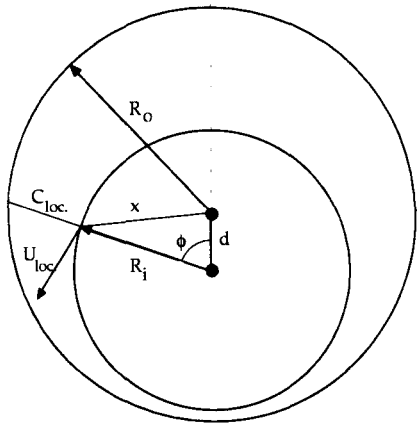

Figure 5.4: Nomenclature as used for the local Taylor number.

This local Taylor number does take eccentricity effects in to account and is based on both the rotational and the whirling velocity. In figure 5.5 this number is calculated for backward whirl at Ω=0.008 rad/s.

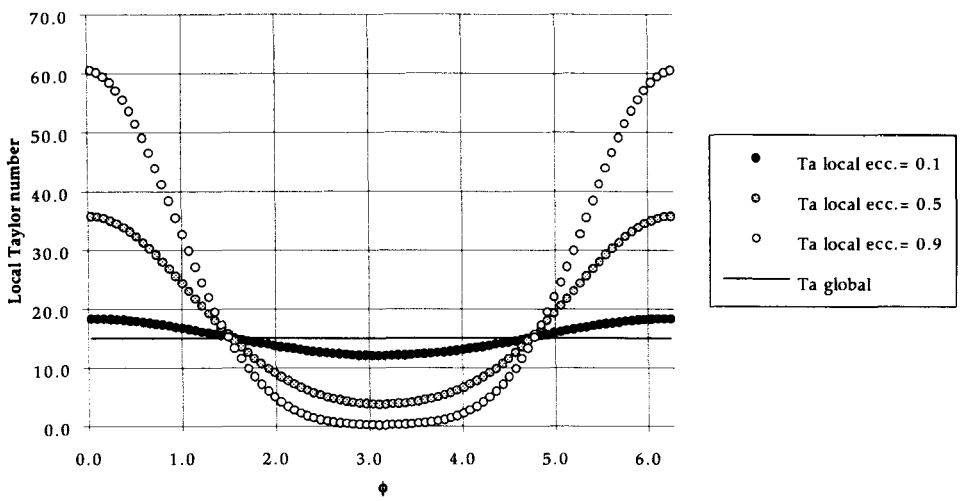

Figure 5.5: Local Taylor number for γ=-1,η=0.63, Ω=0.008 rad/s.

To check if this newly defined Taylor number is an improvement on the global number we will use it to calculate the critical number for the case of an eccentric (non-whirling) rotor and compare this to the data in figure 5.3. The most stable position is found to be at the widest gap position (ϕ=0) [RIT 1968]. For this position the ratio of the local and global Taylor number is:

$$\left.\frac{Ta_{loc.}}{Ta_{glob.}}\right|_{\text{large gap}} = (1+\varepsilon)^{1.5} \tag{5.4}$$

In figure 5.5 both this ratio and the experimental values for $\frac{Ta_{crit.}}{Ta_{glob.crit.}}$ are plotted

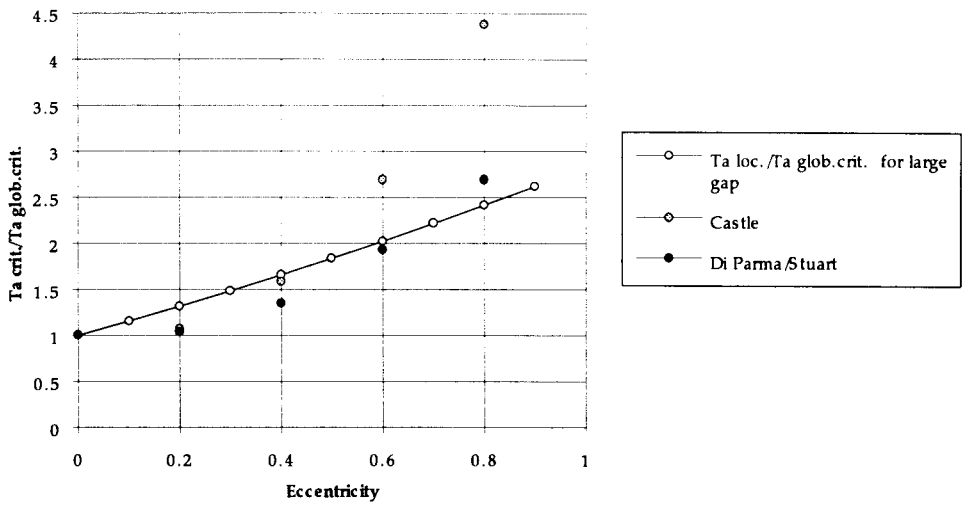

Figure 5.5: Ratio of local and global critical Taylor numbers.

The large gap critical Taylor number resembles the experimental data more accurately. We may therefore conclude that this number is a more accurate description of the flow for the case of an eccentric rotating cylinder. It is plausible that the same considerations are valid for the case of an eccentric whirling cylinder. In fact from the TKE distribution plots in figure 4.17 it is evident that the TKE decreases with increasing ε, thus implying a stabilizing effect. This can however not be further substantiated since no data on critical values are present for this case.

Chapter 6. Conclusions and recommendations.

6.1 Conclusions

A method has been developed for the simulation of the flow in an annulus between an eccentric whirling rotor and a stator using FLUENT V4.2. This is the first (numerical) study, as far as we know, to solve the problem for the whole eccentricity range as well as examining the influence of the non-dimensional parameters η, γ and Ta on the hydrodynamical force and torque on the rotor. The results of this model are independent of the grid size.

The accuracy of the simulations has been established at 3% for laminar flow and 20% for turbulent flow in the concentric case. These accuracy's can not be considered valid for the eccentric cases although they are likely to be a good indication

For low eccentricities good agreement has been found between the lift force obtained from simulations, the Kutta-Zhukhovski lift theorem and data from literature [FRI 1970]. The centrifugal force on the fluid mass displaced by the rotor is found to be not a good approximation of the lift force.

Again for low eccentricities good agreement has been found between the drag force obtained from simulations and the drag force as given by Fritz [FRI 1970]. The simulated drag differs significantly from the drag on a non-rotating circular cylinder and the drag force as given by Iida [IID 1959].

6.2 Recommendations for future research.

The model as described in chapter 2 differs in some critical points from the field situation. The main differences are the assumption of Newtonian fluid, the neglect of axial flow, and the low rotational velocities in the model. These differences should be eliminated in future research in order to obtain a better representation of the actual hydrodynamic force. The model can be extended to include these features without any severe complications. Several tests have already been carried out at higher rotational velocities without encountering major problems.

Furthermore it is recommended to establish the influence of the hydrodynamic forces experimentally. Future research on this subject is justified because it is likely that the magnitude of the forces will be large enough to influence the drillstring dynamics considerably for rotational velocities in the order of 10 rad/s.

References

[AXI 1992] Axisa, F. and Antunes, J., 1992 Flexural vibrations of rotors immersed in dense fluids. Journal of Fluids and Structures 6, 3-21.

[BAT 1987] Batchelor, G.K., 1987. An Introduction to Fluid Dynamics. Cambridge University Press. 11th ed.

[BRE 1976] Brennen, C., 1976. On the flow in an annulus surrounding a whirling cylinder. J. Fluid Mech. 75, part 1, 173-191.

[CAS 1971] Castle, P. and Mobbs, F.R. 1971. Visual observations and torque measurments in the Taylor vortex regime between eccentric rotating cylinders. J. of Lub. Tech., 93, 121

[DIP 1972] DiParma, R.C. and Stuart, J.T. 1972. Non-local effects on the stability of flow between two rotating nonconcentric cylinders. J. Fluid. Mech., 54, 393-415.

[FLU 1993] FLUENT User's guide. Version 4.2. 1993

[FRI 1970] Fritz, R.J., 1970. The effects of an annular fluid on the vibrations of a long rotor Part 1 and 2. J. of Basic Eng. 923-929

[IID 1956] Iida, S., 1956. On the eccentric rotation of a circular cylinder in fluid contained in a circular cylindrical vessel. Proc. of the 6th Jap. Nat. Congress for App. Mech.

[IID 1959] Iida, S., 1959. On the eccentric rotation of a circular cylinder in fluid. Jap. Soc. of Mech. Eng. 2, No. 5.

[JAN 1993] Jansen, J.D., 1993. Nonlinear dynamics of oilwell drillstings. Delft, The Netherlands.

[KAT 1975] Kataoka, K., Doi, H., Hongo T. and Futagawa, M.J. 1975 Taylor vortices and instabilities in circular Couette flows. Chem. Eng. Japan. 8, 472

[KUN 1990] Kundu, P.K., 1990.Fluid mechanics

[LEO 1979] Leonard, B.P. 1979. Stable and accurate convective modelling procedure based on qaudratic upstream interpolation. Computer. Methods in Appl. Mech. Eng., 19, 59-98.

[OTT 1989] Ottino, J.M. 1989. The kinematics of mixing: stretching, chaos, and transport. Cambridge University Press.

[RIT 1968] Ritchie, G.S. 1968. On the stability of viscous flow between eccentric rotating cylinders. J. of Fluid Mech., 32, 131-144.

[ROD 1984] Rodi, W. 1984. Turbulence models and their application in hydraulics, Delft, The Netherlands.

[SCH 1979] Schlichting, H., 1979. Boudary-Layer Theory. McGraw-Hill Series in Mech. Eng., 7th edition.

[SHA 1949] Shaw, M.C. and Macks, E.F. 1949. Analysis and lubrication of bearings. McGraw-Hill Publications in Aeronautical Science. 1st edition.

[TAY 1923] Taylor, G.I., 1923.Stability of a viscous liquid contained between two rotating cylinders. Philosophical Transactions, series A, 233, 289-343.

[URB 1972] Urban, R.L. and Kreuger, E.R.. 1972. On the stability of viscous flow between two rotating nonconcentric cylinders. J. of Franklin Institute 293, 153-172

[WAL 1964] Walston, W.H., Ames, W.F. and Clark, L.G., 1964. Dynamic stability of rotating shafts in viscous fluids. Journal of Applied Mechanics. 291-299

[WAN 1950] Wannier, G.H. 1950. A contribution to the hydrodynamics of lubrication. Quart. of App. Math. 8, 1-32

Appendix 1. List of simulations

This appendix contains a detailed list of all the simulations performed with FLUENT. Figure A1 shows the definition of all the important parameters.

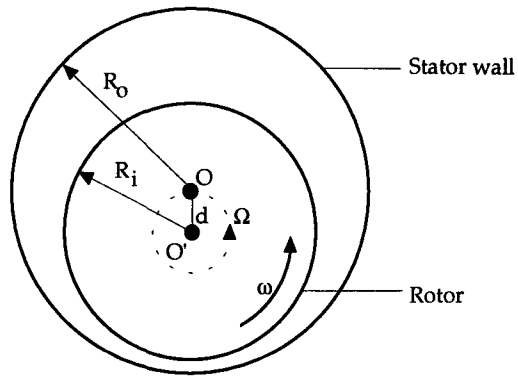

Figure A1: Definition of parameters.

The simulations are divided into 5 sets. For all of these simulations the grid size and the dimensional parameters are listed in the tables A1-A5. In some cases it is more convenient to give a non dimensional parameter.

- Grid independence set. These simulations were carried out to check the grid independence of the results as discussed in section 5.2. The details are given in Table A1.

Grid size	ω [rad/s]	Ω [rad/s]	R_i [m]	R_o [m]	ε	ρ [kg/m^3]	μ [Pas]
45x5	0/0.016	0.008	0.0635	0.1016	0.2/0.5/0.9	998	0.001
45x10	0/0.4	0.2	0.0635	0.1016	0.2/0.5/0.9	998	0.001
180x20	0/0.016	0.008	0.0635	0.1016	0.2/0.5/0.9	998	0.001
180x20	0/0.4	0.2	0.0635	0.1016	0.2/0.5/0.9	998	0.001

Table A1: Grid independence set

- Non-dimensional parameter and scaling factor set. These simulations were carried out to check the validity of the non-dimensional parameters and the scaling factors. The results are discussed in section 5.2. The details are given in Table A2.

Grid size	ω [rad/s]	Ω [rad/s]	R_i [m]	R_o [m]	d	ρ [kg/m^3]	μ [Pas]
90x10	0	0.008	0.0635	0.1016	0.019	998	0.001
90x10	0	0.008	0.0635	0.1016	0.019	1996	0.002
90x10	0	0.004	0.127	0.2032	0.0381	499	0.001

Table A2: Non dimensional and scaling factor set.

For these simulations ε=0.5, η=0.63, γ=0, Ta_{glob}=0.

- Concentric set. These simulations were used to examine the flow and to determine the torque for a concentric rotating cylinder as discussed in section 4.2 and 5.4. The details are given in Table A3.

Grid size	ω [rad/s]	Ω [rad/s]	R_i [m]	R_o [m]	ε	ρ [kg/m^3]	μ [Pas]
90x10	0	0.008	0.0635	0.1016	0	998	0.001
90x10	0	0.02	0.0635	0.1016	0	998	0.001
90x10	0	0.2	0.0635	0.1016	0	998	0.001
90x10	0	0.5	0.0635	0.1016	0	998	0.001

Table A3: Concentric set

- Eccentric laminar set. These simulations were used to determine the influence of ε, η, and γ on the hydrodynamic forces and the torque for laminar flow. The details are given in Table A4.

Grid size	γ	Ω [rad/s]	R_i [m]	R_o [m]	ε	ρ [kg/m^3]	μ [Pas]
90x10	-1/0/1/2	0.008	0.0635	0.1016	0.1/0.3/0.5/0.7/0.9	998	0.001
90x10	-1/1	0.008	0.0711	0.1016	0.1/0.5/0.9	998	0.001
90x10	-1/1	0.008	0.0914	0.1016	0.1/0.5/0.9	998	0.001

Table A4: Eccentric laminar set

- Eccentric turbulent set. These simulations were used to determine the influence of ε and η on the hydrodynamic forces and the torque for turbulent flow. The details are given in Table A5.

Grid size	γ	Ω [rad/s]	R_i [m]	R_o [m]	ε	ρ [kg/m^3]	μ [Pas]
90x10	-1/0/1/2	0.2	0.0635	0.1016	0.1/0.3/0.5/0.7/0.9	998	0.001
90x10	-1/1	0.2	0.0711	0.1016	0.1/0.5/0.9	998	0.001
90x10	-1/1	0.2	0.0914	0.1016	0.1/0.5	998	0.001

Table A5: Eccentric turbulent set

Appendix 2. Colour plot scales

In this appendix the colour spectra for the plots C1-C15 as used in chapter 4 is given. It should be kept in mind, when examining these plots, that the range of the colour scales is adjusted to the maximum and minimum values in each plot. Thus a certain colour in a plot does not represent the same pressure or velocity in another plot. In the surface pressure plots the magnitude of the pressure is also given by the shape of the contour. The contour of the rotor can be considered the zero pressure line for these plots. The colour spectra are given in Figure A2.

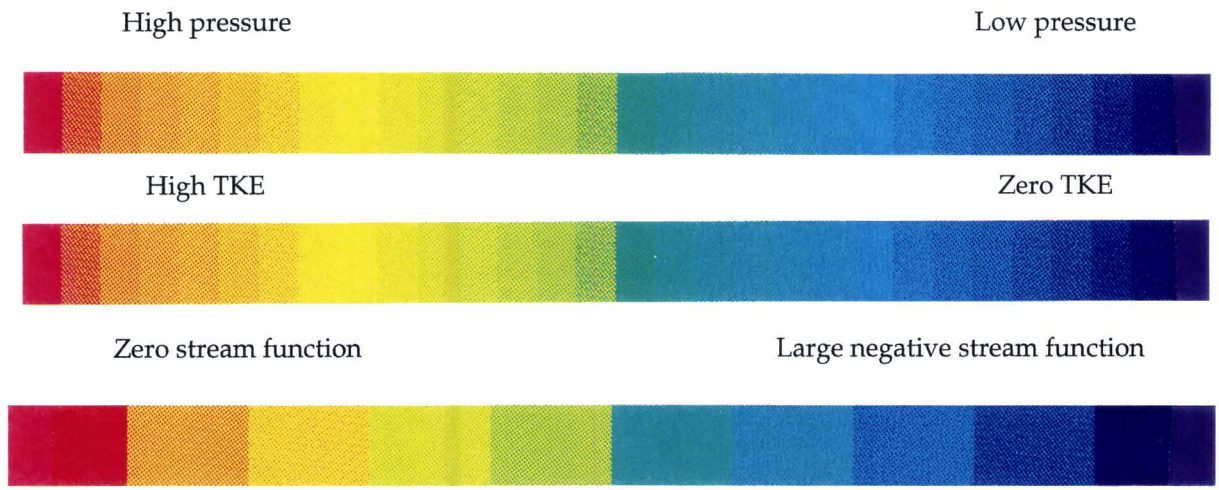

Figure A2: Colour spectra for Figure C1-C15.